Clays and Clay Minerals, 1969, Vol. 17, pp. 115–149. Pergamon Press. Printed in Great Britain

LITHIUM AND POTASSIUM ABSORPTION, DEHYDROXYLATION TEMPERATURE, AND STRUCTURAL WATER CONTENT OF ALUMINOUS SMECTITES*

LEONARD G. SCHULTZ
U.S. Geological Survey, Federal Center, Denver, Colo. 80225

(*Received* 18 *December* 1968)

Abstract—X-ray analysis of Li^+- and K^+-saturated samples, differential thermal analysis (DTA), thermal gravimetric analysis (TGA), and chemical analysis of 83 samples enable a distinction to be made between Wyoming, Tatatilla, Otay, Chambers, and non-ideal types of montmorillonite, and between ideal and non-ideal types of beidellite. The Greene-Kelly Li^+-test differentiates between the montmorillonites and beidellites. Re-expansion with ethylene glycol after K^+-saturation and heating at 300°C depends upon total net layer charge and not upon location of the charge. Wyoming-type montmorillonites characteristically have low net layer charge and re-expand to 17 Å, whereas most other montmorillonites and beidellites have a higher net layer charge and re-expand to less than 17 Å.

Major differences in dehydroxylation temperatures cannot be related consistently to the amount of Al^{3+}-for-Si^{4+} substitution, nor to the amount of Mg, Fe, type of interlayer cations, or particle size. The major factor controlling temperature of dehydroxylation seems to be the amount of structural (OH). Of 19 samples analyzed by TGA, montmorillonites and the one ideal beidellite that give dehydroxylation endotherms on their DTA curves between 650° and 760°C all contain nearly the ideal amount of 4(OH) per unit cell, but the non-ideal montmorillonites and beidellites that give dehydroxylation peaks between 550° and 600°C do not. Non-ideal beidellites contain more than the ideal amount of structural (OH) and non-ideal montmorillonites seem to contain less, although the low temperature of dehydroxylation of the latter could also be due to other structural defects. Change in X-ray diffraction intensity of the 001 reflection during dehydroxylation suggests that the extra (OH) of beidellite occurs at the apex of SiO_4 or AlO_4 tetrahedrons with the H^+ of the $(OH)^-$ polarized toward vacant cation sites in the octahedral sheet.

INTRODUCTION

THE PURPOSE of this paper is to evaluate: (1) the validity of the Greene-Kelly (1955) Li^+-test for distinguishing between montmorillonite and beidellite; (2) the factors that control the expansion characteristics of these minerals when they are K^+-saturated; and (3) the factors that control their different thermal characteristics. An initial group of 28 samples, studied in an effort to understand the effect of various tests on montmorillonitic clays encountered in the Pierre Shale (Schultz, 1966), showed reasonably consistent relationships between chemical composition and the Li^+- and K^+-tests (and also with i.r. absorption, not considered here), but not with temperature of dehydroxylation. In the present expanded group of 83 samples, a particular effort has been made to include more beidellitic and non-ideal (abnormal) montmorillonite types, in the hope of arriving at a consistent explanation of differences in dehydroxylation temperature. Additional tests applied to the current group are Mg^{2+}-glycerol treatment to demonstrate that all samples are smectite and not vermiculite, thermal gravimetric analyses to measure the amount of structural water, and heating X-ray diffractometry to try to determine the location of structural water.

Samples and sources of data

Origin of the 83 samples used is given in Table 1. After some sample names, letters are added in parentheses to distinguish them from samples with otherwise similar names—e.g. (E) obtained from J. W. Earley, (W) from Ward's Scientific establishment, or (GK) from R. Greene-Kelly. Data for two of the samples (nos. 67 and 69) come entirely from the literature and are included for comparison with other closely related samples in the study. The other 81 samples come from many sources and differ considerably in their purity and in reliability of the chemical data for the particular samples studied here. All data for the 81 samples, other than chemical analyses and cation exchange capacity (CEC) values, were obtained for this study on the same homogenized sample, and these data should be directly comparable.

Chemical analyses were made in the U.S. Geological Survey analytical laboratories on 22 of the author's bentonite samples from the Pierre Shale

*Publication authorized by the Director, U.S. Geological Survey.

https://doi.org/10.1346/CCMN.1969.0170302 Published online by Cambridge University Press

Table 1. Source of samples and sample data

1. Clay Spur (E)—original API no. 26 obtained from Earley; bentonite; data from Earley, Osthaus and Milne (1953).
2. Clay Spur (W)—newly collected API no. 26 obtained from Ward's; bentonite; data from API Proj. 49, rept. 7 (Kerr, Hamilton and Pill, 1950, p. 53, 96).
3. Belle Fourche (E)—original API no. 27 obtained from Earley; bentonite; data from Earley, Osthaus and Milne (1953).
4. Belle Fourche (W)—newly collected API no. 27 obtained from Ward's; bentonite; data from API Proj. 49, rept. 7 (Kerr, Hamilton and Pill, 1950, p. 54, 96).
5. Upton (W)—newly collected API no. 25b obtained from Ward's; bentonite; data from API Proj. 49, rept. 7 (Kerr, Hamilton and Pill, 1950, p. 53, 96).
6. Little Rock (E)—original API no. 28 obtained from Earley; bentonite; data from Earley, Osthaus and Milne (1953).
7. Amory (E)—original API no. 22 obtained from Earley; bentonite; data from Earley, Osthaus and Milne (1953).
8. Amory (W)—newly collected API no. 22 obtained from Ward's; bentonite; data from API Proj. 49, rept. 7 (Kerr, Hamilton and Pill, 1950, p. 52, 95).
9. Jenne—obtained by Everett Jenne from American Colloid Co., Belle Fourche, S. Dak.; USGS chemical analysis no. W166948.
10. Jenne-0·25 μ—sample no. 9 < 0·25 μ, Na-citrate-dithionate treated; USGS chemical analysis no. W-166954.
11. Moorcroft (S)—collected by L. G. Schultz from pit in the Clay Spur Bentonite Bed of Mowry Shale in SE$\frac{1}{4}$ sec. 24, T. 50 N., R. 66 W., Crook Co., Wyo., 10 mi. NE. of Moorcroft; USGS chemical analysis no. W166949.
12. Moorcroft (S)-0·25 μ—sample no. 11 < 0·25 μ, Na-citrate-dithionate treated; USGS chemical analysis no. W-166953.
13. Bates Park—obtained from H. H. Murray; from bentonite near Casper, Wyo.; chemical analysis by A. Torok (written commun., 1965).
14. Umiat—obtained from D. M. Anderson; bentonite near Umiat, Alaska; data from Anderson and Reynolds (1966, p. 1452; the structural formula as calculated by Anderson and Reynolds to correspond to a BEC of 100 me/100 g, dry weight).
15. Wyoming (GK)—obtained from R. Greene-Kelly; bentonite from F. W. Berk and Co.; BEC of 0·1 μ material from Greene-Kelly (1955); chemical analysis of Na-saturated < 0·2 μ material from Weir (1965).
16. British Columbia (GK)—obtained from R. Greene-Kelly; bentonite from British Columbia; BEC and layer charge from Greene-Kelly (1955).
17. S57-13A-7—bentonite from DeGrey Member of the Pierre Shale from borehole at Oahe Dam, NE$\frac{1}{4}$ sec. 1, T. 111 N., R. 80 W., Hughes Co., S. Dak.; USGS chemical analysis no. 259537.
18. S57-13C-6b—bentonite from Virgin Creek Member of the Pierre Shale from W. end of Oahe Dam, sec. 30, T. 6 N., R. 31 E., Stanley Co., S. Dak.; USGS chemical analysis no. 259542.
19. S57-22-1—bentonite from the DeGrey Member of the Pierre Shale, sec. 15, T. 6 N., R. 29 E., Stanely Co., S. Dak.; USGS chemical analysis no. 259554.
20. S57-28-10·5—bentonite from Virgin Creek Member of the Pierre Shale from W. end of Wheeler Bridge; SW$\frac{1}{4}$SE$\frac{1}{4}$ sec. 18, T. 96 N., R. 67 W., Gregory Co., S. Dak.; USGS chemical analysis no. 259557.
21. G57-11-0—Ardmore bentonite from Mitten Black Shale Member of the Pierre Shale in SE$\frac{1}{4}$SE$\frac{1}{4}$ sec. 21, T. 7 S., R. 56 E., Carter Co., Mont.; USGS chemical analysis no. 259588.
22. G61-12-53B—bentonite from the Bearpaw Shale near Mosby in SW$\frac{1}{4}$NE$\frac{1}{4}$ sec. 4, T. 14 N, R. 31 E., Garfield Co., Mont.; USGS chemical analysis no. 159752.
23. G61-9A-8b—bentonite from Bearpaw Shale on Porcupine Dome, SW$\frac{1}{4}$SE$\frac{1}{4}$SE$\frac{1}{4}$, sec. 25, T. 7 N., R. 39 E., Rosebud Co., Mont.; USGS chemical analysis no. 159740.
24. G61-6-44—bentonite at top of the Eagle Sandstone in Elk Basin oil field, SW$\frac{1}{4}$SW$\frac{1}{4}$NE$\frac{1}{4}$ sec. 19, T. 58 N., R. 99 W., Park Co., Wyo.; USGS chemical analysis no. 159770.
25. G61-6-48—bentonite at base of the Claggett Formation, same locality as no. 24; USGS chemical analysis no. 159769.
26. G61-2A-3—Sussex bentonite in Cody Shale in Salt Creek oil field, SW$\frac{1}{4}$NW$\frac{1}{4}$ sec. 8, T. 39 N., R. 79 W., Natrona Co., Wyo.; USGS chemical analysis no. 159721.
27. G61-4C-19–bentonite from Bearpaw Shale near Hardin in NW$\frac{1}{4}$SW$\frac{1}{4}$ sec. 9, T. 1 S., R. 35 E., Big Horn Co., Mont.; USGS chemical analysis no. 159728.
28. Tatatilla—U.S. National Museum no. 101836; bentonite? Vera Cruz, Mexico, Ross and Hendricks (1945, sample no. 6). See also Grim and Rowland (1942, p. 755) and Grim and Kulbicki (1961, sample no. 6).
29. April Fool Hill—U.S. National Museum no. C3819; from gold ore shoots, Manhatten, Nev. (Ferguson, 1921); USGS chemical analysis, rept. no. 64 WRC 102.
30. Ely—obtained from R. O. Fournier; altered plagioclase phenocrysts, Liberty porphyry copper mine, Ely, Nev.; chemical analyses (Fournier, 1965, average of analyses 1a and 1b).
31. Greenwood—U.S. National Museum no. R7452; altered pegmatite, Maine; data from Ross and Hendricks (1945, sample no. 28).
32. Rhön—U.S. National Museum no. 103548; altered phonolite, Germany; chemical analysis from Heide (1928); see also Nagelschmidt (1938).
33. Rhön (GK)—obtained from R. Greene-Kelly; BEC from Greene-Kelly (1955); chemical analysis from Weir (1965); both Greene-Kelly and Weir obtained their samples from U. Hofmann (Weiss, Koch and Hofmann, 1955).
34. Otay (E)—original API no. 24 obtained from Earley; bentonite; data from Earley, Osthaus and Milne (1953).
35. Encinitas—U.S. National Museum no. 90473; bentonite 15 mi. from Encinitas, San Diego Co., Calif.; chemical analysis from Melhase (1926) and Ross and Hendricks (1945, sample no. 15); same locality as sample no. 34, and Ross and Hendricks

https://doi.org/10.1346/CCMN.1969.0170302 Published online by Cambridge University Press

Table 1 (*cont.*)

refer to this as an Otay sample; see also Grim and Rowland (1942, p. 755) and Grim and Kulbicki (1961, sample no. 2).

36. Sanders – collected by S. H. Patterson near Sanders, Ariz.; bentonite; locality essentially the same as what has previously been called Cheto (Grim and Kulbicki, 1961, sample no. 1) and Chambers (this report, samples nos. 46, 47); USGS chemical analysis no. W-166950.
37. Sanders-0·25 μ – sample no. 36, $< 0{\cdot}25\ \mu$, Na-citrate-dithionate treated; USGS chemical analysis no. 166955.
38. Cilly–U.S. National Museum no. 13098; bentonite from Cilly, Untersteinmark, Austria; chemical analysis from Ross and Hendricks (1945, sample no. 2) and Kerr (1932).
39. Polkville (W) – newly collected API no. 19 obtained from Ward's; bentonite from near Polkville, Miss.; data from API Proj. 49, rept. no. 7 (Kerr, Hamilton, and Pill, 1950, p. 52, 95), also Grim and Kulbicki (1961, sample 25).
40. Burns (W) – newly collected API no. 21 obtained from Ward's; bentonite from Chisolm Mine near Burns, Miss.; data from API Proj. 49, rept. no. 7 (Kerr, Hamilton, and Pill, 1950, p. 52, 95).
41. Santa Rita (E) – original API no. 30 obtained from Earley; bentonite; data from Earley, Osthaus and Milne (1953).
42. Santa Rita (W) – newly collected API no. 30 labeled API 30a from Bayard, N. Mex., obtained from Ward's; data from API Proj. 49, rept. no. 7 (Kerr, Hamilton and Pill, 1950, p. 51, 96).
43. Helms Park – obtained from H. H. Murray; low-swelling calcium bentonite near Gonzales, Tex.; chemical analysis by A. Torok (written commun., 1965).
44. G58-2-3 – bentonite from the Niobrara Formation, sec. 30, T. 56 N, R. 67 W., Crook Co., Wyo.; USGS chemical analysis no. 155837.
45. S57-37-2 – bentonite from the Sharon Springs Member of the Pierre Shale at Yankton quarry in sec. 17, T. 93 N., R. 56 W., Yankton Co., S. Dak.; USGS chemical analysis no. 155840.
46. Chambers (E) – original API no. 23 obtained from Earley; bentonite; data from Earley, Osthaus and Milne (1953).
47. Chambers (W) – newly collected API no. 23 obtained from Ward's; data from API Proj. 49, rept. no. 7 (Kerr, Hamilton and Pill, 1950, p. 53, 96).
48. Plymouth (E) – obtained from Earley; bentonite west of Plymouth, Utah; data from Earley, Osthaus and Milne (1953).
49. Polkville (E) – original API no. 19 obtained from Earley; bentonite from near Polkville, Miss.; data from Earley, Osthaus and Milne (1953).
50. Lorena (W) – newly collected API no. 20 obtained from Ward's; bentonite from Husband Mine near Lorena, Miss.; data from API Proj. 49, rept. no. 7 (Kerr, Hamilton and Pill, 1950, p. 52, 95).
51. Shoshone – U.S. National Museum no. 96703; bentonite near Shoshone, Amargosa Valley, Calif.; data from Ross and Hendricks (1945, sample no. 3).
52. Amargosa – sample obtained from R. A. Sheppard; "tuff A" from same locality as sample no. 51; USGS chemical analysis no. D100750.
53. S57-18-2 – bentonite from the Sharon Springs Member of the Pierre Shale W. of the Chamberlain bridge, $NW\frac{1}{4}NE\frac{1}{4}$ sec. 17, T. 104 N., R. 71 W., Lyman Co., S. Dak.; USGS chemical analysis no. 259548.
54. G57-22 – bentonite from unnamed member of the Pierre Shale near Elm Springs, $SW\frac{1}{4}SE\frac{1}{4}$ sec. 20, T. 5 N., R. 13 E., Meade Co., S. Dak.; USGS chemical analysis no. 259567.
55. To57-76-6 – bentonite from the Mitten Black Shale Member of the Pierre Shale on North Indian Creek, $NE\frac{1}{4}NE\frac{1}{4}$ sec. 35, T. 12 N., R. 2 E., Butte Co., S. Dak.; USGS chemical analysis no. 259593.
56. G61-20-4 – bentonite from the Two Medicine Formation 7 mi. S. of Choteau in $SW\frac{1}{4}$ sec. 27, T. 23 N., R. 5 W., Teton Co., Mont.; USGS chemical analysis no. 159846.
57. G61-6-105 – bentonite from the Judith River Formation in Elk Basin oil field, $NW\frac{1}{4}SW\frac{1}{4}NW\frac{1}{4}$ sec. 20, T. 38 N., R. 99 W., Park Co., Wyo.: USGS chemical analysis no. 159765.
58. G57-1-45 – Ardmore bentonite from the Sharon Springs Member of the Pierre Shale near Hot Springs in $NE\frac{1}{4}NE\frac{1}{4}$ sec. 31, T. 7 S., R. 7 E., Fall River Co., S. Dak.; USGS chemical analysis no. 259572.
59. G61-13B-29 – bentonite from Clagett Formation near the mouth of the Judith River in $SE\frac{1}{4}NE\frac{1}{4}SW\frac{1}{4}$ sec. 12, T. 22 N., R. 17 E., Fergus Co., Mont.; USGS chemical analysis no. 159817.
60. To57-26-18 – bentonite from Sharon Springs Member of the Pierre Shale near Walhalla, $SE\frac{1}{4}$ sec. 18, T. 163 N., R. 57 W., Cavalier Co., N. Dak.; USGS chemical analysis no. 155836.
61. To57-81B – bentonite from Sharon Springs Member of the Pierre Shale on Elk Creek E. of Piedmont, $NE\frac{1}{4}SE\frac{1}{4}$ sec. 29, T. 4 N., R. 8 E., Meade Co., S. Dak.; USGS chemical analysis no. 155839.
62. G57-1-10 – bentonite near top of Niobrara Formation near Hot Springs, sec. 31, T. 7 S., R. 7 E., Fall River Co., S. Dak.; USGS chemical analysis 155838.
63. Woburn – bentonite sample from the Woburn sands, Bedfordshire, England, obtained from G.P.C. Chambers, Berk and Co., Ltd.; chemical analysis from Mackenzie (1960, 1963).
64. Woburn-0·25 μ – sample no. 63 $< 0{\cdot}25\ \mu$ Na-citrate-dithionate treated; USGS chemical analysis no. W-166952.
65. Atzcapozalco – sample no. 67, reanalyzed, USGS chemical analyses rept. no. 64WRC102.
66. Atzcapozalco, purified – sample no. 67, Na-citrate-dithionate treated; USGS chemical analysis no. W-166956.
67. Atzcapozalco (R-H) – U.S. National Museum no. R7591; altered basalt, Mexico; chemical analysis from Ross and Hendricks (1945, sample 22).
68. Redhill (GK) – sample obtained from Greene-Kelly (1955); bentonite from Redhill, Surrey, England; chemical composition from Weir (1965).
69. Black Jack (W-G) – data from Weir and Greene-Kelly (1962) are given for comparison with sample no. 70.
70. Black Jack – U.S. National Museum no. R4762; vein clay from Black Jack Mine, Carson District, Owyhee Co., Idaho; chemical analysis from Ross and

https://doi.org/10.1346/CCMN.1969.0170302 Published online by Cambridge University Press

Table 1 (*cont.*)

Hendricks (1945, sample no. 49); see also Ross and Shannon (1926, p. 94).

71. Beidell—U.S. National Museum no. 93239; gouge clay from Beidell, Colo.; chemical data from Ross and Hendricks (1945, sample no. 44); see also Grim and Rowland (1942, p. 802).
72. Wagon Wheel Gap—U.S. National Museum no. 94963; gouge clay from fluorite mine near Wagon Wheel Gap, Colo.; chemical analysis from Ross and Hendricks (1945, sample no. 47); also Grim and Rowland (1942, p. 802).
73. JH-10—$< 2\,\mu$ fraction from claystone from the Petrified Forest Member of the Chinle Formation N. of Joseph City, Ariz.; chemical data from Schultz (1963, p. C6).
74. P-10—$< 2\,\mu$ fraction from claystone from Petrified Forest Member of the Chinle Formation near Paria, Utah; data from Schultz (1963, p. C6) and USGS chemical analysis no. W-166951.
75. Cameron(W)—newly collected API no. 31 obtained from Ward's; claystone from Petrified Forest Member of the Chinle Formation N. of Cameron, Ariz.; data from API proj. 49, rept. no. 7 (Kerr, Hamilton and Pill, 1950, p. 56, 97).
76. Castle Mountain—obtained from H. Heystek; hydrothermally altered Tertiary tuff 12 mi. E. of Ivanpah, Calif.; chemical data from Heystek (1963, p. 163).
77. Rectorite—collected by Frank Williams from roadcut in state highway 7 near Jessieville, Garland Co., Ark.; data from Brown and Weir (1963); see also Brackett and Williams (1891), W. F. Cole and J. S. Hosking (*in* Mackenzie, 1957, p. 263–64), Bradley (1950) and Kodama (1966).
78. Pontotoc—collected by H. A. Tourtelot from railroad cut near Pontotoc, Miss., described by Ross and Stephenson (1939); chemical analysis from Ross and Hendricks (1945, sample no. 50).
79. Tem-Pres B-1—synthetic beidellite with 1·34 Na/unit cell from Tem-Pres Research, Inc., Code A44/145; structural formula assumed from composition of charge used in hydrothermal bomb (Koizumi and Roy, 1959).
80. Tem-Pres B-2—synthetic beidellite like no. 79 but with 0·66 Na/unit cell; Code A35/112.
81. Tem-Pres B-3—like no. 80; Code A56/23.
82. Tem-Pres B-4—like no. 80; Code B35/112.
83. Tem-Pres B-5—like no. 80; Code B56/25.

and related rocks and on 13 other samples of particular interest. These analyses are unquestionably comparable with all other data for these samples. A shortcoming for many Pierre samples is presence of impurities in the unfractionated sample analyzed, for which corrections were necessary before calculation of the structural formulas. Published chemical analyses were used for all other samples. Of these, 17 samples were obtained directly from the authors, and the published chemical data should apply directly to data obtained on these samples during this study. Examples are Earley's (Earley, Osthaus, and Milne, 1953) reanalyzed Na^+-saturated size-fractions of original API standards.

Twenty-five chemical analyses of samples not obtained directly from authors may not be representative of the samples used in this study, because the lumps of clay obtained are not homogenized splits of the originally analyzed samples. Many such samples obtained from the U.S. National Museum, such as those of Ross and Hendricks (1945), are of particular historical interest. Also, several API samples obtained from Ward's Scientific Establishment in 1965 are included because they are still widely used standards and generally seem to conform closely to the originals, even though they have been newly collected from near the original sites and thus may not be identical with samples described in API Report 49 (Kerr *et al.* 1949, 1950). These newly collected samples are designated as such.

Five beidellite samples are synthetic. Their structural formulas are assumed from the compositions of the charges in the hydrothermal bombs in which they were crystallized (Koizumi and Roy, 1959), and their chemical compositions (Table 2, nos. 79–83) are calculated from these structural formulas.

Structural formulas

Structural formulas calculated by the method of Ross and Hendricks (1945) from the chemical compositions in Table 2 are given in Table 3 with other analytical data. The calculated structural formula of sample no. 1, Clay Spur(E), is $K_{0\cdot01}Na_{0\cdot80}Ca_{0\cdot02}(Al_{3\cdot06}Fe^{3+}_{0\cdot42}Mg_{0\cdot52})(Al_{0\cdot32}Si_{7\cdot68})O_{20}(OH)_4$. The sum of octahedral cations is 4·00 per unit cell, the ideal sum for dioctahedral clays. The net layer charge due to substitution of cations within the structure is $-0\cdot85$ per unit cell, which is balanced by the $+0\cdot85$ charge on the interlayer cations. These do not exactly balance for some of the other samples due to rounding of the calculated numbers, in which case the charge on the interlayer cations is taken as the net layer charge. Substitution of 0·32 Al^{3+} for Si^{4+} accounts for 38 per cent of the net layer charge, and this is referred to as the tetrahedral charge. The 62 per cent of the net layer charge that is due to Mg^{2+}-for-Al^{3+} substitution will be referred to as the octahedral charge.

The structural formulas are not inerrant, but should be considered as useful and, one hopes, realistic transformations of the chemical analyses for evaluation in conjunction with all other data. The accuracy of a structural formula depends on several factors (Kelley, 1955): (1) the accuracy of the chemical analysis, which for most samples is quite good, although alkalies are particularly suspect in older analyses; (2) the accuracy of corrections made for crystalline impurities; (3) the absence of unrecognized amorphous impurities; (4) the validity of assumptions made in assigning elements to different structural positions, e.g. Al^{3+} may be

https://doi.org/10.1346/CCMN.1969.0170302 Published online by Cambridge University Press

octahedral, tetrahedral, or interlayer, and Mg^{2+} may be octahedral or interlayer; and (5) the validity of the assumption that a total negative charge per unit cell $[O_{20}(OH)_4]^{-44}$ must be balanced by +44 charges on cations, which is true only if the amount of structural (OH) actually is 4·00 per unit cell. Several types of data can help control uncertainties in the assumptions and corrections involved in the structural formulas.

Cation exchange capacity (CEC) sould be directly proportional to layer charge. For this paper, all CEC values have been converted to milli-equivalents per 100 g (me/100 g) of *ignited* material, which should be about 140 times the layer charge per unit cell $[O_{20}(OH)_4]$. However, capacities determined by different methods, by different workers, and at different times may differ considerably, and all interlayer cations of every sample are not exchangeable. In some literature, the values are not specified to be on an air-dried, oven-dried, ignited basis; in such cases a 100°C oven-dried basis is assumed.

The CEC values reported for most samples average about 130 times the calculated net layer charge, which is considered a reasonably good agreement with the structural formulas. However, several small groups of samples have reported exchange capacities that conflict strongly with calculated net layer charges. In most such cases, the structural formulas seem to be the more reliable measure of layer charge. For one example, the four predominantly Ca^{2+} API samples (Table 3, nos. 39, 40, 42 and 47) all are reported to have exceptionally high CEC values of 159 to 174 me/100 g. The values are much higher than indicated by their calculated layer charges and should be in the CEC range of vermiculite (D. M. C. MacEwan, *in* Brown, 1961, p. 145). However, they expand fully to 18 Å when Mg^{2+} saturated and glycerol treated, indicating that they are montmorillonites and not vermiculites (G. F. Walker, *in* Brown, 1961, pp. 315–316), and thus that the reported CEC values likely are too high. For a second example, Ross and Hendricks (1945, p. 39) give CEC values that are all consistently lower than expected from the structural formulas (Table 3, nos. 28, 31, 35, 51 and 67); newer chemical analyses of samples from three of these same localities (nos. 34, 52 and 65) are in much closer agreement with the structural formulas than with the CEC figures. For a third example, two Pierre and one Niobrara samples (nos. 53, 61 and 62) and the Pontotoc sample (no. 78) have CEC values that are too low for the calculated layer charges, apparently because they contain considerable gibbsite-like interlayer material in which the Al^{3+} ions are not entirely exchangeable. Also, relatively low CEC values for samples nos. 73, 74 and 75 are reasonable when due consideration is given to non-exchangeable K^+ in their illite interlayers, and the low capacity of the rectorite (no. 77) is due to the interlayered paragonite layers.

An exception to CEC values being less reliable than calculated layer charge seems to be the group of three API Wyoming-type bentonites (Table 3, nos. 2, 4 and 5). All are reported to have reasonably normal CEC values of 92 to 106 me/100 g of ignited material, but their calculated net layer charges are only 0·42, 0·46 and 0·35, respectively. These charges are only a little more than half that expected from reported CEC values, and only about half the layer charge calculated for all other Wyoming-type samples. Two of Earley's samples from these same localities (Table 3, nos. 1 and 3) support the CEC values of samples 2 and 4. Therefore, the structural formulas given in Table 3 for these three API Wyoming-type samples were calculated with assumed sodium contents large enough to give layer charges corresponding to their reported CEC values. Except for these three, the structural formulas calculated by the method of Ross and Hendricks (1945) will be used as the primary measure of net layer charge.

Other types of data also can help in derivation of an appropriate structural formula or in evaluation of a calculated formula. Determination of exchangeable cations gives a value for the amount of interlayer Mg^{2+}, but the value may be only a minimum because all interlayer Mg^{2+} may not be exchangeable. Exchangeable H^+ probably indicates presence of interlayer Al^{3+}, as the latter almost invariably accompanies the former in interlayer positions. Appreciable amounts of interlayer Mg^{2+} or Al^{3+} also are indicated by X-ray data from heated clays. Both cations tend to form moderately stable interlayer hydroxyl-water complexes that are not volatilized at 300°C like normal interlayer water, and the basal spacing is correspondingly high. Inasmuch as clays with abundant interlayer Al^{3+} give acid clay–water slurries and those with Mg^{2+} give alkaline slurries, a pH determination was combined with X-ray evidence for stable interlayer complexes as the basis for transferring Mg^{2+} or Al^{3+} ions in excess of the ideal 4·00 octahedral cations into interlayer positions of the structural formulas (Table 3). Such samples with no excess of octahedral cations have been treated in different ways. If the total charge on the calculated interlayer cations seemed reasonable, the structural formula is given as calculated, but with a question mark in the interlayer Mg^{2+} or Al^{3+} column on Table 3. If the total for interlayer cations seemed exceptionally low, as for sample no. 60, the structural formula is recalculated with interlayer H^+ (or H_3O^+). The structural formulas for such samples with deficient totals for octahedral cations probably should be regarded with more than normal suspicion.

An attempt was made to remove all interlayer

https://doi.org/10.1346/CCMN.1969.0170302 Published online by Cambridge University Press

https://doi.org/10.1346/CCMN.1969.0170302 Published online by Cambridge University Press

Table 2. Chemical analyses (wt. %)

Sample No.	1	2	3	4	5	6	7	8	9	10
Name	Clay Spur (E)	Clay Spur (W)	Belle Fourche (E)	Belle Fourche (W)	Upton (W)	Little Rock (E)	Amory (E)	Amory (W)	Jenne	Jenne (0·25 μ)
SiO_2	61·47	60·96	61·12	58·53	57·49	60·69	59·30	51·52	58·4	54·7
Al_2O_3	22·17	18·27	23·10	19·61	20·27	22·40	20·40	17·15	18·5	19·9
Fe_2O_3	4·32	2·83	4·37	3·10	2·92	5·67	7·74	5·65	3·6	2·5
FeO		0·14		0·13	0·19			0·32	0·00	0·96
MgO	2·73	2·96	2·50	2·65	3·18	1·87	2·40	2·80	2·4	2·4
CaO	0·14	0·10	0·24	0·25	0·23	0·00	0·03	1·72	1·2	0·07
Na_2O	3·18	1·44	2·90	1·68	1·32	2·50	2·52	0·15	1·9	3·8
K_2O	0·03	0·31	0·04	0·31	0·28	0·13	0·66	0·85	0·32	0·05
$H_2O(-)$		6·78		7·89	7·63			11·22	6·9	9·2
$H_2O(+)$	6·02	6·56	5·84	6·21	6·85	6·61	6·25	8·55	6·3	5·1
TiO_2	0·09	0·08	0·09	0·12	0·12	0·19	0·76	0·48	0·14	0·13
P_2O_5	0·02		0·05			trace	0·14		0·03	0·56
MnO	trace		trace			0·00	0·07		0·02	0·00
CO_2									0·30	0·30
Sum	100·17	100·43	100·25	100·48	100·48	100·06	100·27	100·41	100	100
Impurities (per cent)	2 Crist.	10 Qtz.		2 Qtz. 2 Crist.		2 Crist.	2 Hem.	2 Qtz. 2 Gyp.	6 Qtz. 1 Crist. 1 Plag.	

https://doi.org/10.1346/CCMN.1969.0170302 Published online by Cambridge University Press

Table 2. (*cont.*)

Sample No.	11	12	13	14	15	16	17	18	19	20
Name	Moorcroft (S)	Moorcroft (S) (0·25 μ)	Bates Park	Umiat	Wyoming (GK)	B.C. (GK)	S57-13A-7	S57-13C-6b	S57-22-1	S57-28-10·5
SiO_2	59·4	54·9	53·5	55·99	64·8		57·6	56·67	56·6	53·39
Al_2O_3	19·8	20·3	21·2	18·92	24·6		19·1	18·86	19·7	20·21
Fe_2O_3	3·1	1·9	3·74	3·38	4·25	2·2	3·3	3·29	5·0	2·30
FeO	0·28	1·6			0·21		1·0	2·09	0·5	0·27
MgO	2·4	2·4	2·27	3·08	2·83	2·54	2·6	2·37	2·7	2·47
CaO	0·30	0·10	0·71	1·61	0·00		1·4	1·47	2·4	1·84
Na_2O	2·7	3·4	1·75	nd	3·15		2·2	1·52	2·0	0·19
K_2O	0·33	0·13	0·20	0·08	0·04	0·00	0·64	0·55	0·89	0·08
$H_2O(-)$	7·0	9·5	15·25	nd			7·0	6·15	4·6	11·22
$H_2O(+)$	4·3	5·3		nd	ignited		4·5	5·14	4·1	6·19
TiO_2	0·11	0·13	0·19	0·15			0·24	0·22	0·63	0·41
P_2O_5	0·15	0·08					0·07	0·07	0·20	0·02
MnO	0·00	0·00					0·02	0·07	0·07	0·02
CO_2	0·08	0·18	0·13				0·41	0·73	0·20	0·06
Sum	100	100	99·0		99·88		100	100	100	100
Impurities	8 Qtz. 5½ Plag. 1 K-sp.					30 Crist.	2 Plag. 2 K-sp. 1 Calc.	2 siderite	10 Biot. 10 Plag. 1 Gyp.	1 Qtz. 2 Jar.

https://doi.org/10.1346/CCMN.1969.0170302 Published online by Cambridge University Press

Table 2. (*cont.*)

Sample No.	21	22	23	24	25	26	27	28	29	30
Name	G57-11-0	G61-12-53B	G61-9A-8b	G61-6-44	G61-6-48	G61-2A-3	G61-4C-19	Tatatilla	April Fool Hill	Ely
SiO_2	42·8	55·7	56·7	54·4	55·9	57·6	58·5	52·09	51·7	50·05
Al_2O_3	15·7	21·0	20·5	22·6	19·4	18·3	16·4	18·98	19·4	21·8
Fe_2O_3	9·1	4·3	3·8	4·0	4·8	4·2	2·7	0·06	0·05	0·83
FeO	0·10	0·30	0·46	0·42	0·28	0·18	0·21		0·20	
MgO	1·8	2·8	2·9	2·1	2·6	3·0	4·0	3·80	3·6	3·2
CaO	2·7	0·84	0·82	1·6	2·0	0·97	1·5	3·28	2·6	2·3
Na_2O	0·62	1·8	2·5	2·6	2·5	2·9	1·7		0·06	0·06
K_2C	0·62	0·38	0·43	0·54	0·31	0·16	0·18		0·00	0·58
$H_2O(-)$	9·8	6·1	4·9	6·0	5·7	6·2	7·3	14·75	15·3	13·0
$H_2O(+)$	6·0	6·0	4·8	4·6	4·9	5·1	5·3	7·46	7·0	7·9
TiO_2	0·17	0·35	0·29	0·58	0·69	0·59	0·23	0·00	0·00	
P_2O_5	0·04	0·12	0·13	0·26	0·15	0·07	0·04		0·01	
MnO	0·02	0·00	0·01	0·01	0·03	0·02	0·08	0·06	0·01	
CO_2	0·07	0·00	0·12	0·00	1·0	0·73	1·0		0·08	
Sum	100	100	100	100	100	100	100	100·48	100	99·75
Impurities	5 Gyp. 15 Jar.	6 Plag. 4 Biot.	4 Plag. 4 Biot. 2 Qtz. 1 Jar.	5 Plag. 6 Biot. 2 Kaol.	3 Plag. 3 Biot. 2 Calc.	1 Plag. 2 Biot. 4 Clino. 2 Calc.	10 Crist. 2 Biot.		1 Qtz.	5 musc.

https://doi.org/10.1346/CCMN.1969.01703O2 Published online by Cambridge University Press

Table 2. (*cont.*)

Sample No.	31	32	33	34	35	36	37	38	39	40
Name	Greenwood	Rhön	Rhön (GK)	Otay (E)	Encinitas	Sanders	Sanders (0·25 μ)	Cilly	Polkerville (W)	Burns (W)
SiO_2	54·28	49·21	64·0	63·04	50·30	51·4	55·2	52·43	50·95	51·18
Al_2O_3	22·94	22·61	29·0	18·44	15·96	15·4	17·0	15·95	16·54	16·30
Fe_2O_3	0·24	0·43	0·21	1·20	0·86	1·5	1·6	1·42	1·36	2·20
FeO						0·04	0·20	0·10	0·26	0·23
MgO	2·92	2·13	3·03	7·30	6·53	5·0	5·0	5·02	4·65	4·41
CaO	3·18	1·95		0·08	1·24	2·3	0·09	2·97	2·26	2·12
Na_2O	0·08	0·45	3·98	3·40	1·19	0·30	3·1		0·17	0·17
K_2O		trace	0·05	0·02	0·45	0·12	0·26		0·47	0·38
$H_2O(-)$	7·82	14·34			23·61	16·2	11·0	13·96	15·01	15·02
$H_2O(+)$	8·70	9·34	ignited	6·47		7·4	6·0	7·60	8·28	8·29
TiO_2	0·06			0·14		0·22	0·29	0·08	0·32	0·28
P_2O_5				0·05		0·21	0·11	0·08		
MnO				0·01		0·17	0·00		0·01	0·01
CO_2						< 0·05	0·10			
Sum	100·24	100·47	100·27	100·15	100·14	100	100	100·13	100·28	100·59
Impurities	2 Qtz. 20 Bdll.	20 Bdll.								

https://doi.org/10.1346/CCMN.1969.0170302 Published online by Cambridge University Press

Table 2. (*cont.*)

Sample No.	41	42	43	44	45	46	47	48	49	50
Name	Santa Rita (E)	Santa Rita (W)	Helms Park	G58-2-3	S57-37-2	Chambers (E)	Chambers (W)	Plymouth (E)	Polkville (E)	Lorena (W)
SiO_2	65·21	55·11	56·1	55·9	55·4	61·16	49·91	58·60	63·42	47·64
Al_2O_3	19·13	15·56	21·8	17·4	18·0	20·38	17·20	20·64	19·44	17·79
Fe_2O_3	1·07	0·94	0·92	2·3	1·2	3·66	2·17	4·89	1·87	3·35
FeO		0·13					0·26			0·32
MgO	4·57	4·37	3·57	4·2	3·3	4·52	3·45	4·00	5·00	2·63
CaO	0·04	2·21	2·29	0·70	2·4	0·14	2·31	0·64	0·11	1·23
Na_2O	3·90	0·13	1·16	0·26	0·08	3·70	0·14	3·00	3·46	0·12
K_2O	0·14	0·10	0·04	0·44	0·18	0·04	0·28	0·07	0·08	0·26
$H_2O(-)$		13·14	13·5	11·0	11·6		15·77			19·25
$H_2O(+)$	5·83	8·65		6·6	6·5	6·40	7·70	7·63	6·15	6·78
TiO_2	0·14	0·07	0·22	0·93	0·64	0·37	0·24	0·57	0·32	0·12
P_2O_5	trace			0·02	0·02	0·03		0·02	0·04	
MnO	0·03	0·05		0·00	0·02	0·03	0·04	0·03	0·00	
CO_2			0·50		0·05					
Sum	100·06	100·46	100·35	100	100	100·43	99·47	100·09	99·89	99·49
Impurities	5 Crist.	5 Crist.	7 Kaol. 1 Calc.	2 Crist.	1 Qtz. 1 Jar.			1 Crist.		

https://doi.org/10.1346/CCMN.1969.01703O2 Published online by Cambridge University Press

Table 2. (*cont.*)

Sample No.	51	52	53	54	55	56	57	58	59	60
Name	Shoshone	Amargosa	S57-18-2	G57-22	To57-76-6	G61-20-4	G61-6-105	G57-1-45	G61-13B-29	To57-26-18
SiO_2	54·58	56·69	47·12	52·3	52·7	57·5	58·2	51·2	51·2	54·9
Al_2O_3	16·44	18·61	20·79	16·9	17·1	16·9	17·6	18·6	17·2	19·5
Fe_2O_3	2·59	2·41	2·65	4·7	3·7	3·7	4·1	3·2	4·0	1·6
FeO	0·11	0·16	0·56	0·6	1·0	0·24	0·43	0·20	0·28	
MgO	4·90	5·14	3·06	4·4	4·2	3·0	2·8	3·6	4·3	3·1
CaO	0·72	0·56	0·81	2·7	1·4	1·3	1·5	1·8	2·1	0·11
Na_2O	3·02	1·43	0·70	0·64	0·30	2·4	2·2	0·26	0·61	0·09
K_2O	0·81	0·47	0·36	0·68	0·12	0·25	0·44	0·08	0·28	0·22
$H_2O(-)$	11·10	7·47	11·62	9·2	13·1		7·9	11·2	11·7	12·7
$H_2O(+)$	5·49	5·95	7·30	5·9	5·4		4·5	6·4	6·5	6·7
TiO_2	0·18	0·20	0·24	0·42	0·56	0·48	0·33	0·58	0·42	0·50
P_2O_5		0·02	0·09	0·12	0·05	0·07	0·01	0·08	0·08	0·05
MnO		0·01	0·03	0·06	0·02	0·01	0·01	0·03	0·03	0·01
CO_2		0·01	0·03	0·88		0·36	0·21	0·12	1·1	0·00
Sum	99·94	99·77	100	100	100	100	100	100	100	100
Impurities			2 Gyp. 5 Jar.	8 Biot. 2 Calc. 2 Gyp.	1 Biot.	10 Qtz. 3 Plag. 3 Biot. 1 Calc.	7 Qtz. 5 Plag. 5 Biot.	4 Gyp. 3 Jar.	4 Plag. 3 Biot. 2 Calc. 2 Clino.	

https://doi.org/10.1346/CCMN.1969.0170302 Published online by Cambridge University Press

Table 2. (*cont.*)

Sample No.	61	62	63	64	65	66	67	68	69	70
Name	To57-81B	G57-1-10	Woburn	Woburn 0·25 μ	Atzcapozalco	Atzcapozalco purified	Atzcapozalco (R-H)	Redhill (GK)	Black Jack (W-G)	Black Jack
SiO_2	54·9	51·2	50·30	52·7	50·2	52·9	50·44	64·7	59·30	45·32
Al_2O_3	19·8	23·5	14·86	14·2	16·7	17·9	16·26	18·6	36·11	27·84
Fe_2O_3	3·7	2·0	8·86	10·4	5·0	4·8	5·38	8·12	0·50	0·80
FeO			0·35	0·88	0·10	0·20	trace	0·25		
MgO	3·0	2·2	3·06	2·2	4·0	2·9	3·92	4·32	0·10	0·16
CaO	0·09	0·72	2·07	0·10	0·95	0·12	0·72		0·02	2·76
Na_2O	0·12	1·2	0·00	3·2	0·58	2·9		3·30	3·98	0·10
K_2O	0·16	0·56	0·04	0·16	0·38	0·27		0·04	0·11	0·12
$H_2O(-)$	11·4	9·4	15·06	10·4	15·3	10·2	16·00			22·64
$H_2O(+)$	6·1	6·7	6·20	5·4	6·1	6·3	6·30	ignited	ignited	
TiO_2	0·27	1·0	0·13	0·39	0·59	0·98	0·42			
P_2O_5	0·15	0·11		0·07	0·02	0·35				
MnO	0·01	0·01	0·00	0·00	0·01	0·00				
CO_2	0·00			< 0·05	0·00	< 0·05				
Sum	100	100		100	100	100	99·44	99·33	100·12	99·74
Impurities		4 Jar. 5 Kaol.	1 Qtz. 2 Hem.					50 Chambers-type		

https://doi.org/10.1346/CCMN.1969.0170302 Published online by Cambridge University Press

Table 2. (*cont.*)

Sample No.	71	72	73	74	75	76	77	78	79	80-83
Name	Beidell	Wagon Wheel Gap	JH-10	P-10	Cameron (W)	Castle Mtn.	Rectorite	Pontotoc	Tem-Pres B-1	Tem-Pres B-2 to 5
SiO_2	47·28	48·05	49·6	51·2	54·37	55·80	55·2	46·95	53·36	60·00
Al_2O_3	20·27	23·01	20·0	18·5	17·79	28·60	38·7	27·26	36·30	32·32
Fe_2O_3	8·68	6·67	5·2	5·8	7·14	0·41	0·59	2·26		
FeO			0·16	0·00	0·27			0·32		
MgO	0·70	2·14	2·2	3·3	1·20	2·03	0·00	1·39		
CaO	2·75	1·52	2·2	1·0	1·83	2·23	0·33	0·00		
Na_2O	0·97	0·21	0·56	2·5	0·26	0·09	4·40	0·20	5·54	2·78
K_2O	trace	1·04	0·65	1·3	2·49	0·48	0·11	0·36		
$H_2O(-)$	19·72	10·46	18·8	9·4	6·31	9·70		11·10		
$H_2O(+)$		6·14		6·1	6·79		ignited	10·55	4·80	4·90
TiO_2			0·51	0·52	0·56	0·26		0·00		
P_2O_5			0·38	0·12				0·03		
MnO			0·04	0·00				0·01		
CO_2			0·12	< 0·05	0·32					
Sum	100·37	99·24	100	100	99·50	99·60	99·33	100·43	Calculated from assumed structural formulas (Table 3)	
Impurities		20 Kaol.	5 Qtz.	4 Qtz.	8 Qtz.					

Impurities, in per cent: Qtz.-quartz; Crist.-cristobalite; Plag.-plagioclase; K-sp.-potassium feldspar; Gyp.-gypsum; Calc.-calcite; Jar.-jarosite; Kaol.-kaolinite; Clino.-clinoptilolite; Biot.-biotite; Musc.-muscovite; Hem.-hematite; Bdll.-beidellite.

Table 3. Structural

Sample	Structural formula (Numbers indicate atoms per formula)										Net layer charge	
	Interlayer					Octahedral					Tetrahedral		Per cent Tetrahedral
	K^+	Na^+	Ca^{2+}	Mg^{2+}	Al^{3+}	Al^{3+}	Fe^{3+}	Fe^{2+}	Mg^{2+}	Total	Al^{3+}	Total	
Wyoming-type													
1 – Clay Spur (E)	0·01	0·80	0·02			3·06	0·42		0·52	4·00	0·32	0·85	38
2 – Clay Spur (W)	0·06	0·70	0·02			3·04	0·32	0·02	0·67	4·05	0·24	0·80[1]	30
3 – Belle Fourche (E)	0·01	0·71	0·03			3·11	0·42		0·47	4·00	0·31	0·78	40
4 – Belle Fourche (W)	0·06	0·58	0·03			3·11	0·34	0·02	0·57	4·04	0·20	0·70[1]	29
5 – Upton (W)	0·05	0·64	0·03			3·06	0·30	0·02	0·65	4·03	0·18	0·75[1]	24
6 – Little Rock (E)	0·02	0·64	0·00			3·10	0·56		0·36	4·02	0·34	0·66	51
7 – Amory (E)	0·11	0·64	0·01			2·99	0·50		0·48	3·97	0·18	0·77	23
8 – Amory (W)	0·17	0·05	0·29			2·91	0·43		0·66	4·04	0·25	0·80	31
9 – Jenne	0·06	0·54	0·12			3·02	0·41	0·00	0·55	3·98	0·25	0·84	30
10 – Jenne −0·25 μ	0·01	1·05	0·01			3·06	0·27	0·11	0·51	3·94	0·26	1·08	24
11 – Moorcroft (S)	0·04	0·72	0·00			3·07	0·38	0·04	0·58	4·07	0·35	0·76	46
12 – Moorcroft −0·25 μ	0·03	0·93	0·02			3·09	0·20	0·19	0·51	3·99	0·28	1·00	28
13 – Bates Park	0·03	0·48	0·11			3·17	0·40		0·48	4·05	0·39	0·73	54
14 – Umiat						2·96	0·36		0·64	3·96	0·16	0·84	19
15 – Wyoming (GK)		0·72				3·13	0·38	0·02	0·50	4·03	0·31	0·72	42
16 – B. C. (GK)												0·68	22
17 – S57-13A-7	0·05	0·55	0·10			2·95	0·36	0·12	0·57	4·00	0·12	0·80	15
18 – S57-13C-6b	0·10	0·41	0·20			3·00	0·34	0·09	0·49	3·92	0·10	0·91	11
19 – S57-22-1	0·00	0·46	0·19			3·06	0·47	0·00	0·35	3·88	0·04	0·84	5
20 – S57-28-10·5	0·00	0·04	0·30		0·10[2]	3·33	0·13	0·02	0·54	4·02	0·21	0·72	29
21 – G57-11-0	0·00	0·14	0·21		0·02	3·24	0·25	0·01	0·50	4·00	0·14	0·62	23
22 – G61-12-53B	0·00	0·42	0·05	0·10		3·13	0·44	0·01	0·42	4·00	0·25	0·72	35
23 – G61-9A-8b	0·00	0·67	0·00			3·15	0·30	0·05	0·55	4·07	0·24	0·67	36
24 – G61-6-44	0·00	0·70	0·19			3·17	0·38	0·02	0·31	3·88	0·45	1·08	42
25 – G61-6-48	0·00	0·67	0·07			2·98	0·48	0·01	0·47	3·95	0·18	0·81	22
26 – G61-2A-3	0·00	0·76	0·00			2·89	0·46	0·02	0·63	4·00	0·12	0·76	16
27 – G61-4C-19	0·00	0·54	0·00	0·18		2·93	0·31	0·01	0·74	4·00	0·18	0·90	20
Tatatilla-type													
28 – Tatatilla	0·00	0·00	0·52			3·15	0·01	0·00	0·85	4·01	0·20	1·04	19
29 – April Fool Hill	0·00	0·07	0·42	0·07		3·22	0·01	0·03	0·74	4·00	0·22	1·05	21
30 – Ely	0·00	0·02	0·39	0·13		3·28	0·10		0·62	4·00	0·44	1·06	41
31 – Greenwood	0·00	0·02	0·48			3·24	0·01		0·74	3·99	0·27	0·99	27
32 – Rhön	0·00	0·16	0·29	0·08		3·46	0·03		0·51	4·00	0·36	0·90	40
33 – Rhön (GK)	0·01	0·90	0·00	0·04		3·49	0·02		0·49	4·00	0·51	0·99	51
Otay-type													
34 – Otay (E)	0·00	0·83	0·01	0·17		2·69	0·11		1·20	4·00	0·05	1·18	4
35 – Encinitas	0·09	0·30	0·20	0·20		2·69	0·10		1·31	4·10	0·22	1·19	18
36 – Sanders	0·01	0·08	0·39	0·14		2·78	0·18	0·01	1·03	4·00	0·05	1·15	5
37 – Sanders– 0·25μ	0·05	0·86	0·02	0·08		2·81	0·17	0·03	0·99	4·00	0·07	1·11	7
38 – Cilly	0·00	0·00	0·48	0·10		2·76	0·16	0·01	1·07	4·00	0·07	1·16	6
39 – Polkville (W)	0·09	0·05	0·37	0·14		2·87	0·16	0·04	0·93	4·00	0·14	1·16	12
40 – Burns (W)	0·07	0·05	0·35	0·11		2·81	0·26	0·03	0·90	4·00	0·14	1·04	13
41 – Santa Rita (E)	0·02	1·00	0·01			2·97	0·10		0·90	3·97	0·02	1·04	2
42 – Santa Rita (W)	0·02	0·04	0·37	0·09		2·91	0·12	0·02	0·95	4·00	0·00	0·98	1
43 – Helms Park	0·01	0·33	0·24	0·04		3·15	0·10		0·75	4·00	0·16	0·90	17
44 – G58-2-3	0·08	0·07	0·11	0·19		3·06	0·22		0·74	4·00	0·00	0·75	0
45 – S57-37-2	0·03	0·03	0·38		0·10[2]	3·12	0·10		0·73	3·95	0·00	0·92	0
Chambers-type													
46 – Chambers (E)	0·01	0·91	0·02			2·84	0·35		0·85	4·04	0·22	0·96	23
47 – Chambers (W)	0·06	0·05	0·38	0·05		2·95	0·25	0·04	0·76	4·00	0·21	0·97	22
48 – Plymouth (E)	0·01	0·77	0·09			2·81	0·49		0·79	4·09	0·40	0·96	41
49 – Polkville (E)	0·02	0·85	0·02			2·89	0·17		0·94	4·00	0·00	0·91	0
50 – Lorena (W)	0·06	0·04	0·22	0·17		3·08	0·41	0·04	0·47	4·00	0·36	0·88	41
51 – Shoshone	0·15	0·82	0·11	?		2·65	0·28	0·02	1·05	4·00	0·14	1·19	12
52 – Amargosa	0·08	0·38	0·08	0·20		2·87	0·25	0·02	0·86	4·00	0·16	1·02	16
53 – S57-18-2	0·02	0·21	0·06		0·31	3·21	0·01	0·04	0·74	4·00	0·68	1·28	37

https://doi.org/10.1346/CCMN.1969.0170302 Published online by Cambridge University Press

formulas and other data

Li⁺-test				K⁺	DTA			CEC	020 reflection
Per cent Illite	Per cent Beidellite	Per cent drop 9·6 Å	18/9·6 ratio	300°C glycol 001 spacing	Dehydroxylation peak temp.	Ending (Fig. 4)	Firing product	me/100 g ignited weight	peak height c/s
	15	18		17 −	720	W	a	110	115
	28	32		17 −	710	W	a	106	115
	35	25		17 +	710	W	a	100	145
	13	17		17 +	715	W	nd	92	115
	12	12		17 +	725	W	a	102	130
	37	31		17 +	705	W	a	95	160
	21	15		17 −	700	W	a	93	115
	20	25		17 −	710	W	a	96	90
	13	13		17 −	715	W	nd		140
	20	13		16·4	725	W	a		
	10	9		17 −	720	W	a		150
	12	8		16·4	720	W	a		
	18	18		17 −	705	W	a		110
	16	23		17 −	710	W	a		120
	20	22		17 −	715	W	nd	100	120
	20	20		17 +	715	W	nd		135
	19	17		17 +	720	W	a		120
	16	11		17 +	715	W	a		140
	16	13		17 +	700	W	a	97	135
	31	21		17 +	705	L	a	101	190
	20	15		17 +	705	L	nd		110
	20	16		17 +	705	C	S		130
	15			17 +	710	W	a		160
	48	49	0·13	16·0	715	W	a		140
	12	13		17 −	700	W	a		130
	12	12		17 −	715	W	a		130
	11	12		16·4	700	C-W	S		140
	14	16		15·2	725	S	C, M	87	180
	15	13		15·2	735	S	M		180
	18	25		13·6	715	S	M	144	170
	20	22		16·4	730	D	a	91	130
	25	30		14·2	710	D	a		200
	55	58	0·57	14·0	720	S	nd	124	150
	12	8		13·8	650	S	S	137	110
	10	8		13·6	650	S	Q	105	140
	15	8		13·8	670	S	Q		140
	15	8		13·7	665	S	Q		115
	10	8		14·0	660	S	Q		130
	7	0		15·0	690	S	Q	174	150
	10	5		16·0	685	S	Q	171	130
	10	10		13·8	690	S	Q	132	180
	8	6		13·6	680	S	Q	174	180
	7	8		16·3	690	S	Q		115
	10	9		14·5	690	S	Q	108	155
	5	3		14·3	690	S	Q	111	170
	20	23		13·4	675	C	a	132	170
	20	28		15·2	680	C	a	159	130
	33	30		14·2	660	C	a	129	110
	22	25		13·8	680	C	a	129	110
	39	50	0·1	16·4	675	C	a	127	95
	13	11		13·8	680	C	S	106	165
	15	22		13·5	675	C	S		200
	24	33		14·2	670	C	a	109	125

https://doi.org/10.1346/CCMN.1969.0170302 Published online by Cambridge University Press

Table 3

Sample	Structural formula (Numbers indicate atoms per formula)											Net layer charge	
	Interlayer					Octahedral					Tetrahedral		Per cent Tetrahedral
	K^+	Na^+	Ca^{2+}	Mg^{2+}	Al^{3+}	Al^{3+}	Fe^{3+}	Fe^{2+}	Mg^{2+}	Total	Al^{3+}	Total	
Chambers-type, *cont.*													
54 – G57-22	0·00	0·15	0·20	0·15		2·85	0·45	0·03	0·67	4·00	0·14	0·85	16
55 – To57-76-6	0·00	0·09	0·15	0·25		2·85	0·42	0·09	0·65	4·00	0·16	0·89	18
56 – G61-20-4	0·00	0·71	0·11			2·90	0·41	0·01	0·65	3·97	0·20	0·93	22
57 – G61-6-105	0·00	0·65	0·16			2·92	0·44	0·03	0·54	3·93	0·15	0·97	15
58 – G57-1-45	0·00	0·06	0·06		0·26	2·96	0·19	0·03	0·82	4·00	0·15	0·96	16
59 – G61-13B-29	0·00	0·07	0·08	0·33		2·86	0·46	0·02	0·66	4·00	0·23	0·89	26
60 – To57-26-18	0·04	0·03	0·02		0·80[2]	3·14	0·17		0·66	3·97	0·15	0·91	16
61 – To57-81B	0·03	0·03	0·02	0·40[2]	0·11	3·00	0·37		0·63	4·00	0·20	0·83	24
62 – To57-1-10	0·06	0·36	0·12		0·35[2]	3·47	0·00		0·51	3·98	0·45	1·01	45
Non-ideal montmorillonite													
63 – Woburn			0·35		?	2·53	0·79	0·05	0·73	4·10	0·23	0·70	33
64 – Woburn – 0·25 μ	0·03	0·91	0·02		?	2·21	1·15	0·11	0·49	3·96	0·25	0·98	25
65 – Atzcapozalco	0·07	0·18	0·16	0·21		2·71	0·58	0·01	0·70	4·00	0·30	0·99	30
66 – Atzcapozalco, purified	0·05	0·83	0·02	0·02		2·83	0·53	0·03	0·61	4·00	0·26	0·96	27
67 – Atzcapozalco, (R-H)	0·00	0·00	0·12	0·27		2·75	0·62		0·63	4·00	0·21	0·78	27
68 – Redhill (GK)	0·01	0·78	0·00			2·51	0·74	0·03	0·78	4·06	0·15	0·79	19
Beidellites													
69 – Black Jack (W-G)	0·02	0·90	0·00			3·96	0·04		0·02	4·02	1·04	0·92	100
70 – Black Jack	0·03	0·03	0·45			3·93	0·09		0·04	4·06	1·08	0·96	100
71 – Beidell		0·28	0·45	?		2·80	0·99		0·15	3·94	0·82	1·18	70
72 – Wagon Wheel Gap	0·25	0·08	0·30	0·13		2·59	0·94		0·47	4·00	0·72	1·19	61
73 – JH-10	0·13	0·17	0·38	0·11		2·93	0·63	0·02	0·42	4·00	0·85	1·28	66
74 – P-10	0·26	0·75	0·17			2·60	0·67	0·00	0·76	4·03	0·75	1·35	56
75 – Cameron (W)	0·51	0·08	0·32			2·73	0·85	0·04	0·29	3·91	0·61	1·23	50
76 – Castle Mtn.	0·08	0·02	0·31	0·13		3·69	0·04		0·27	4·00	0·71	0·98	72
77 – Rectorite	0·01	0·94	0·04			4·07	0·05		0·00	4·11	1·39	1·03	100
78 – Pontotoc	0·07	0·05	0·00		0·41	3·40	0·25	0·04	0·30	4·00	0·99	1·33	74
79 – Tem-Pres B-1		1·32				4·00					1·32	1·32	100
80 – Tem-Pres B-2		0·66				4·00					0·66	0·66	100
81 – Tem-Pres B-3		0·66				4·00					0·66	0·66	100
82 – Tem-Pres B-4		0·66				4·00					0·66	0·66	100
83 – Tem-Pres B-5		0·66				4·00					0·66	0·66	100

DTA firing products: a-amorphous; Q-beta quartz; S-spinel; C-cordierite; M-mullite; nd-not determined; ?-see text

[1]Increased Na^+ assumed to correspond with CEC; see text for explanation.

[2]H^+.

[3]Paragonite.

[4]Pyrophyllite.

[5]590°C equal in size to 670°C peak.

[6]555°C equal in size to 725°C peak.

Al^{3+} and Mg^{2+} from five of the author's samples (nos. 10, 12, 37, 64 and 66) by Na^+-citrate-dithionate treatment (Jackson, 1958, p. 168). A much milder NaCl treatment was used by Earley to Na^+-saturate his samples (nos. 1, 3, 6, 7, 34, 41, 46 and 48). The treatments did not remove all interlayer Mg^{2+}or Al^{3+} from samples nos. 34, 37 and 66. In addition, the dithionate procedure removed considerable other crystalline clay material and reduced some iron in the clay structure from ferric to ferrous, thereby increasing the layer charge (compare samples nos. 9 with 10, and nos. 11 with 12). Nevertheless, all results for each of these treated samples should be comparable, because the chemical analyses and all tests were made after the treatments.

The smectites used in this study are classified into seven groups based on their composition, on the amount and distribution of their layer charge, and on their thermal behavior, properties which are revealed by chemical analyses, Li^+- and K^+-treatment, DTA, and TGA. Group names used throughout this paper are Wyoming, Tatatilla, Otay, Chambers, and non-ideal montmorillonite, and ideal and non-ideal beidellite. The names will be familiar to most readers from the literature

https://doi.org/10.1346/CCMN.1969.0170302 Published online by Cambridge University Press

(*cont.*)

Li⁺-test				K⁺	DTA			CEC	020 reflection
Per cent Illite	Per cent Beidellite	Per cent drop 9·6 Å	18/9·6 ratio	300°C glycol 001 spacing	Dehydroxylation peak temp.	Ending (Fig. 4)	Firing product	me/100 g ignited weight	peak height c/s
	22	19		15·8	670	C	nd	102	105
	20	13		14·2	670	C	nd		120
	18	15		14·7	690	C	a		120
	13	15		14·7	675	C	a		115
	25	18		16·0	675	L	M, S		150
	16	12		16·4	680	C	M, S		115
	15	12		14·5	680	L	M	100	200
	14	17		16·4	685	L	S	93	170
	50	50	1·0	15·2	680	L	M, S	116	170
	35			15·8	560	X	a		70
	24	32		15·8	590	X	a		70
	28	31		14·7	560	C	a		90
	32	?		15·8	590	C	a		90
								75	
	12	19		15·8	[5]	C	nd	107	90
	100				560	X		130	
	100		3·5	13·2	560	X	M		165
35	60		?	15·0	550	X	a		85
20	50		1·0	16·0	550	X	nd		85
Tr	89		1·6	13·8	580	C	a	135	90
15	55	0·50	0·9	13·4	590	D	a	157	75
35	55	0·53	0·9	12·8	585	C	a	91	90
	72		1·9	13·6	560	S	M	110	115
50[3]	50			17 –	600	none	nd	54	80
	85			15·0	575	W	a	75	80
	85		3·0	17 –	760	W	M		200
20[4]	80		2·0	15·2	[6]	C	M		165
	100		3·5	17 +	730	X	M		130
35[4]	65		1·0	14·5	[6]	D	M		180
	100		3·6	17 –	725	X	M		110

except for the use of "ideal" and "non-ideal". "Ideal" indicates a dehydroxylation peak temperature on the DTA curve in the 650–760°C range that is generally considered normal for montmorillonite. "Non-ideal" indicates a lower dehydroxylation temperature in the range of 550–600°C. Thus, a non-ideal montmorillonite corresponds to an "abnormal" montmorillonite of Cole and Hosking (*in* Mackenzie, 1957, p. 256). "Abnormal" has not been used in this paper to avoid possible confusion in extending the term to beidellites, thereby either having "abnormal" refer to the high temperature form of beidellite and the low temperature form of montmorillonite, or, if "abnormal" were redefined to refer to the low temperature form of both minerals, of having the extremely rare high temperature form of beidellite as the normal form.

Li⁺-TEST OF GREENE-KELLY

The net negative layer charge of beidellite is due to Al^{3+}-for-Si^{4+} substitution in the tetrahedral sheet, and that of montmorillonite, mainly to Mg^{2+}-for-Al^{3+} substitution in the octahedral sheet. The Li⁺-test of Greene-Kelly (1955) is said to distinguish between the two clays on the basis of the degree of re-expansion with glycerol after a Li⁺-saturated sample has been collapsed by heating. In both clays about one-third of the possible octahedral cation sites are not occupied. The theory of the Li⁺-test is that Li⁺ ions are sufficiently small that when a clay is heated they can enter the layer structure. If the net layer charge is in the octahedral sheet, the Li⁺ will occupy previously vacant octahedral cation sites, thereby neutralizing the net layer charge and making the clay non-expanding.

https://doi.org/10.1346/CCMN.1969.0170302 Published online by Cambridge University Press

If the net layer charge is in the tetrahedral sheet where there are no vacant cation sites, the Li^+ will not go into the structure and the clay will retain its expansibility.

The Li^+-test was applied in this study using X-ray diffractometer traces of an oriented aggregate rather than the camera procedure originally described. A thin oriented clay layer on an inch-long porous ceramic tile was saturated with Li^+ by sucking 3N LiCl through the clay layer and tile sealed above a vacuum. The tile was set aside for 2 hr in contact with 3N LiCl, and then washed free of excess salt by sucking distilled water through it several times. After air-drying, the slide was heated at 200°C overnight and X-rayed (CuKα) from 2 to 21°2θ at 2°/min and again from 17 to 21°2θ at $\frac{1}{2}$°/min and a smaller scale factor. The slide was then covered with glycerol overnight, excess glycerol was then removed, and each slide was X-rayed at the same settings with the recorder traces superimposed over the 200°C traces so that changes in *d*-values or peak intensities are readily apparent.

Interlayer water is absent from both montmorillonite- and beidellite-like layers after Li^+-saturation and heating at 200°C, so that both have 001 *d*-values of about 9·6 Å and 002 *d*-values of about 4·8 Å. Saturation with glycerol expands the beidellite-like layers to an 001 *d*-value of about 18 Å. The 004 of any re-expanded beidellite layers at 4·5 Å combines with the 4·8 Å 002 of unexpanded montmorillonite layers to shift the *d*-value of the 002/004 mixed-layer montmorillonite/beidellite reflection. The proportion of layers that re-expand is determined from the shift in *d*-value by using MacEwan's 002/004 curve (*in* Brown, 1961, p. 417) modified to correspond to 9·6/18 Å mixed-layering. The shift rather than the *d*-value itself was used because the *d*-value was not uniform for different samples after the 200°C heat treatment, but ranged from 4·75 to 4·85 Å. The reflection at 4·26 Å from quartz in the tile served as an internal spacing standard. Glycerol liquid rather than vapor at 110°C was used, because the vapor did not re-expand known beidellites uniformly to 18 Å, whereas the liquid did. Presence of originally non-expanding illite, paragonite, or pyrophyllite layers in several of the beidellite samples (Table 3) was determined from the first three basal reflections of the original glycol- and Mg^{2+}-glycerol-treated sample.

The site of net layer charge from structural formulas is compared in Fig. 1 with the proportion of re-expansible beidellite-like layers. Mixed-layered illite and paragonite layers in several beidellite samples are counted as though they were re-expanding beidellite-like layers because such micas most likely are tetrahedrally charged and would expand were they not keyed together by K^+ or Na^+ before the Li^+-treatment. The two synthetic beidellites (nos. 80 and 82, Table 3) mixed-layered with non-expanding pyrophyllite are nevertheless plotted at 100 per cent re-expansion on the basis that all originally expansible layers remain so after the Li^+-treatment. The assumed 100 per cent tetrahedral charge cannot apply to the uncharged pyrophyllite, and therefore it is excluded from the proportions.

Five samples are exceptionally far outside the general range of scatter on Fig. 1, as follows: (1) Sample no. 79 is a synthetic beidellite. Its assumed structural formula indicates that all of its net layer charge is in the tetrahedral layer, but only 85 per cent of the layers re-expand. However, judged from the four synthetic beidellites (nos. 80–83) some of the assumed structural formulas for the synthetic beidellites must not be correct. Samples 80–83 all crystallized from identical materials, but their markedly different properties (Table 3) indicates that the crystalline phases cannot have identical compositions. Possibly the montmorillonitic behavior of 15 per cent of the layers in synthetic beidellite no. 79 is due to vacant Al^{3+} sites in some octahedral sheets, the layer charge from which can be neutralized by the Li^+. (2) Sample no. 75 plots considerably above the average curve on Fig. 1. This sample is the API no. 31 from Cameron, Arizona, newly collected from a thick and mineralogically variable sedimentary unit in the Chinle Formation. Thus, there is a maximum possibility that the newly collected Cameron sample is different from the originally analyzed sample. The marked deficiency in the total of 3·91 octahedral cations also suggests some inaccuracy in the calculated structural formula. (3) Sample no. 49 from Polkville, Miss., has none of its calculated net layer charge in the tetrahedral sheet, but nevertheless 22 per cent of its layers re-expand. The sample analyzed for this study gives a DTA curve typical of a Chambers-type sample, but the published DTA curves and chemical analyses are typical of an Otay-type sample (Earley, Osthaus and Milne, 1953; Kerr, Kulp and Hamilton, 1949, Fig. 13; also compare sample 39, Table 3, newly collected API-19). Sample no. 49 evidently has been mislabeled. (4) The structural formula of sample no. 11 is brought into question by its purified counterpart, sample no. 12 (Table 3), which shows a more normal relationship between charge and re-expansion. (5) No explanation for the plotted position of sample no. 13 is apparent.

The many possible errors in the compositional data probably could account for much of the observed scatter on Fig. 1, in addition to the five exceptionally incongruent samples. However, the test itself must cause some of the scatter. The only circumstance in which it could measure the exact

https://doi.org/10.1346/CCMN.1969.0170302 Published online by Cambridge University Press

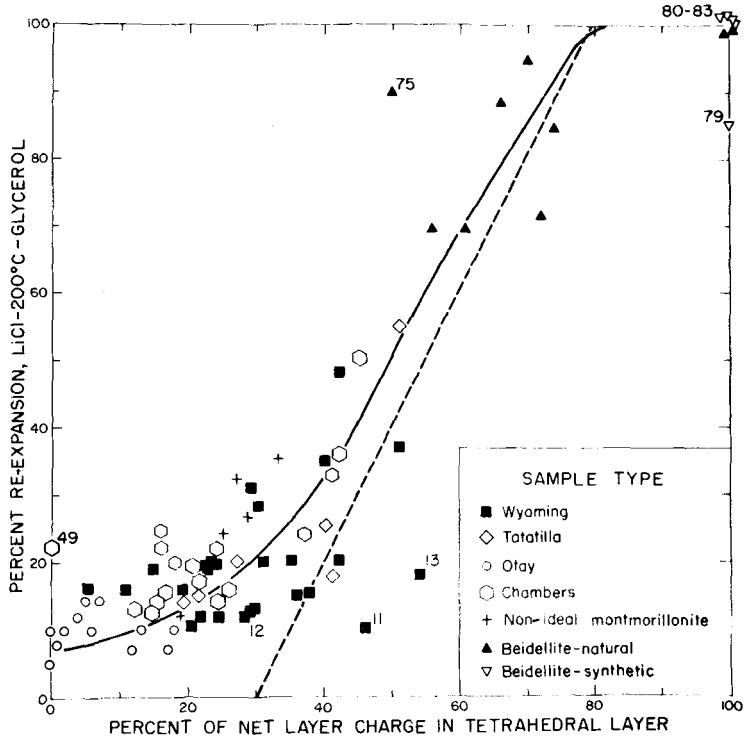


Fig. 1. Re-expansion of Li^+-treated smectite derived from the position of the 4·8/4·5 Å 002/004 montmorillonite/beidellite peak. Dashed line is Greene-Kelly's curve (1955). Numbered samples are discussed in text.

charge distribution would be if inhomogeneity of charge distribution were exactly the same in all samples, which seems improbable. The charge must not be uniformly distributed in most clays, or none could be partly re-expanding, with some layers that behave like montmorillonite and others like beidellite (Greene-Kelly, 1955, p. 613); all samples would be either entirely expanding or entirely non-expanding. However, although two clays may each have 20 per cent average tetrahedral charge, if nearly all of the charge is concentrated in about 20 per cent of the silica sheets of the first sample, and 10 per cent is concentrated and 10 per cent dispersed in the second, then the first would be 20 per cent re-expanding but the second probably would be only 10 per cent re-expanding. Thus some inconsistency in results from the Li^+-test should be inherent.

Both the Li^+-test itself and compositional inaccuracies likely cause some of the scatter of data points on Fig. 1, but it is difficult to say which causes more. Perhaps the most reasonable evaluation is that the Li^+-test gives a valid approximate indication of octahedral versus tetrahedral distribution of the net layer charge accurate to 10 per cent, or possibly no better than 20 per cent. Even such an approximate measure is quite valuable, as it is obtained with relative ease and may be more reliable than layer charge distribution calculated from chemical data, particularly of impure material. The test will be used as a cross-check for structural formulas in parts of this paper that follow.

An alternate method for interpreting the degree of re-expansion after glycerol-treatment is illustrated in Fig. 2. As the proportion of beidellite-like re-expansible layers increases from 0 to 35 per cent, the 001 peak of the glycerol treated sample does not shift appreciably from 9·6 Å, but the reflection broadens and decreases notably in intensity relative to the 001 peak from the fully collapsed clay (Fig. 2a). The baseline rises in the 15–20 Å region but no peak normally develops. Only rarely does a very broad peak at 14–15 Å appear at about 35 per cent re-expansible layers. With a larger proportion of re-expansible layers, the decrease in the 9·6 Å peak intensity continues, the peak starts to shift to a perceptibly smaller *d*-value, and at a content of about 40–45 per cent re-expansible layers a broad peak develops at 18–19 Å (Fig. 2b). At 50–60 per cent re-expansion the ~ 19 Å

https://doi.org/10.1346/CCMN.1969.0170302 Published online by Cambridge University Press

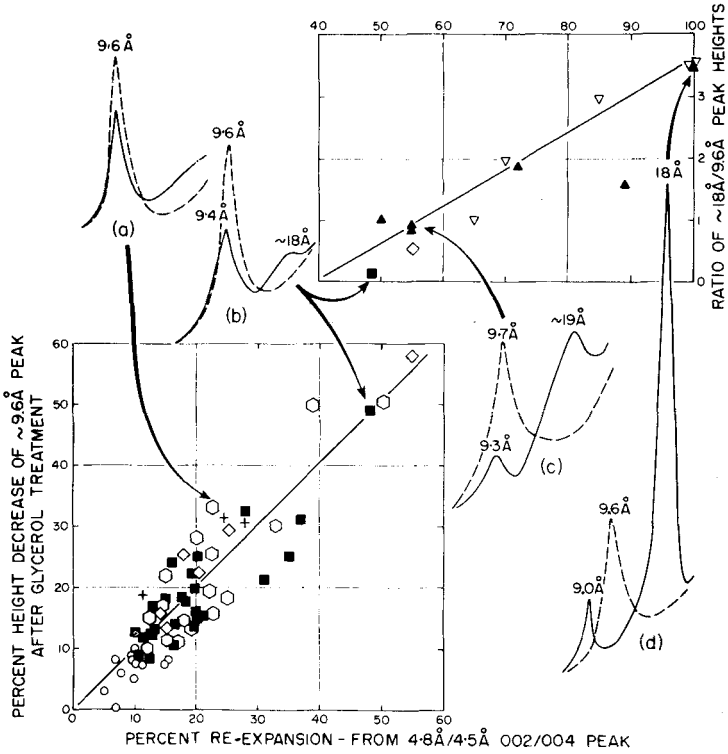


Fig. 2. Relative intensities of basal reflections related to re-expansion of Li^+-200°C-glycerol treated smectite. (a)–(d) are X-ray diffractometer traces: - - - Li^+-treated, 200°C; ——— same slide after glycerol saturation. Sample symbols as on Fig. 1.

peak height nearly equals the original 9·7 Å peak height of the heated clay (Fig. 2c). At 100 per cent re-expansion the sharp 18 Å peak has about three times the intensity of the original 9·6 Å reflection (Fig. 2d). The alternate method is particularly useful for the impure clays in most rocks for which the illite 002 and/or the chlorite 003 may obscure the commonly weak 002/004 montmorillonite–illite/beidellite mixed-layer reflection, and the 001 illite obscures the 001/002 mixed-layer reflection used by Greene-Kelly (1955). A plot of net layer charge in the tetrahedral layer against relative intensities of basal reflections (not shown) resembles Fig. 1 closely.

K^+-SATURATION AND LAYER CHARGE

Some authors (Wear and White, 1951; Weaver, 1958; Mackenzie, 1963; Harward and Brindley, 1965; Kerns and Mankin 1968) have suggested that the effect of K^+-saturation on montmorillonite depends primarily on the site of net layer charge within a layer structure, and possibly also may indicate the origin of the clay. The reasoning is that the expansible clays derived from mica will inherit a large net layer charge in the tetrahedral sheet near the interlayer cations, which will strongly attract and tend to fix K^+-ions, making the layers nonexpanding. Those clays derived from nonmicaceous material, like volcanic glass, tend to remain expanding because their net layer charge is mainly in the octahedral sheet of the structure far from the exchangeable cations. Other authors (Barshad, 1954; Grim and Kulbicki, 1961; Weir, 1965) report expansion after K^+-saturation related more to the total amount of net layer charge than to the position of the charge within the layer.

Potassium saturated slides for this study were prepared with 1N KCl in the same manner as the Li^+ slides; heated at 300°C for ½ hr; treated overnight in ethylene glycol vapor at 60°C; and X-rayed. The 001 spacings from different samples ranged from 17 Å with well developed higher orders, indicating no decrease in expansibility, to about 13 Å. Spacings are given on Table 3 and are related to layer charge in Fig. 3. The symbols indi-

https://doi.org/10.1346/CCMN.1969.0170302 Published online by Cambridge University Press

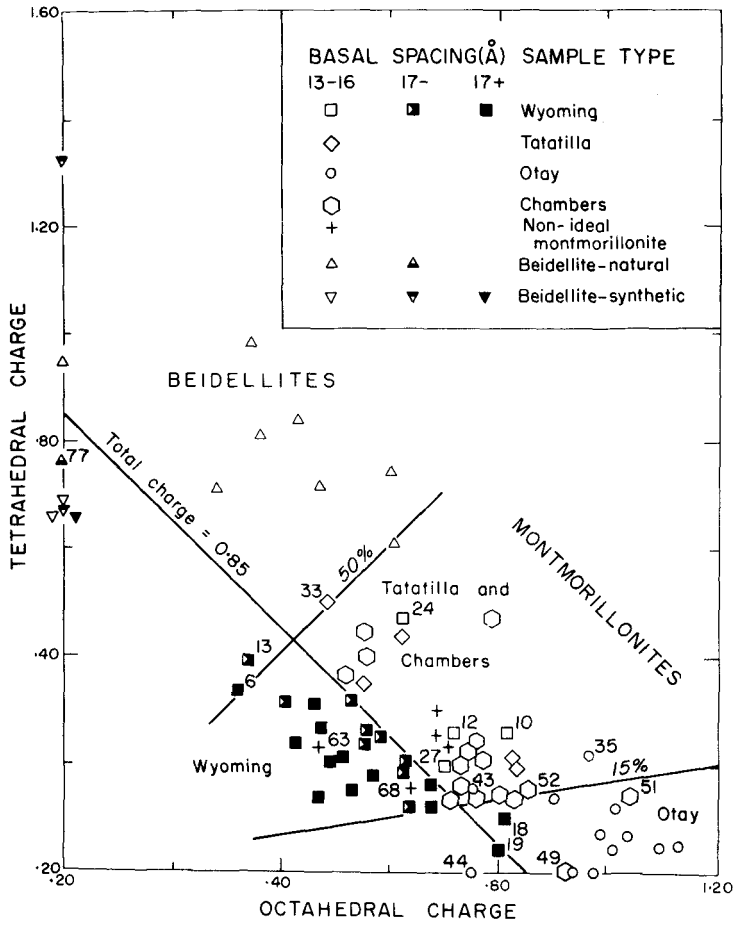


Fig. 3. Re-expansion with ethylene glycol after K^+-saturation and heating at 300°C, related to position and amount of net layer charge per unit cell. Tetrahedral charge is tetrahedral Al^{3+} and octahedral charge is difference between total net layer charge and tetrahedral Al^{3+} (Table 3). The 17− indicated an 001 at 17 Å but poorly developed irrational higher basal orders; 17+ indicates a sharp, rational 00*l* sequence. Lines labeled 15 and 50 per cent correspond to these percentages of the total net layer charge in the tetrahedral sheet. Numbered samples are discussed in the text.

cate the type of smectite and approximate degree of re-expansion after the K^+-treatment.

Re-expansion of K^+-saturated montmorillonites with a net layer charge that is less than half in the tetrahedral sheet, plotted below the 50 per cent line on Fig. 3, is closely related to total net layer charge. Most samples with a total net layer charge less than 0·85/unit cell re-expand to 17 Å; most of those with a greater net layer charge do not. Within the 17 Å re-expanding range, most that do not give a series of sharp basal orders (17−) have total net layer charges between 0·75 and 0·85/unit cell. Those giving a sharp basal series (17+) mostly have total net layer charges less than 0·75.

The relation of total net layer charge to re-expansion on the beidellite side of Fig. 3 appears not nearly so consistent as on the montmorillonite side, mainly due to the synthetic beidellites. However, as previously discussed in connection with the Li^+-test, the assumed structural formulas of the synthetic beidellites are not reliable. Aside from the synthetic beidellites, all but one of the natural beidellites have net layer charges well above 0·85/unit cell and have limited re-expansion similar to

https://doi.org/10.1346/CCMN.1969.0170302 Published online by Cambridge University Press

montmorillonites with similar net layer charges. The only natural beidellite in the group that re-expands almost completely (17—) is rectorite (no. 77, Table 3), which is calculated to have an average net layer charge of 1·03/unit cell. However, rectorite is a 1/1 regularly mixed-layered paragonite (Na mica)/beidellite. The paragonite layers must certainly have a net layer charge greater than the average for the rectorite, and the expanding beidellite layers must then have a charge correspondingly less than the average. The reported CEC of the sample is 54 me/100 g, which, if attributed entirely to the expanding half of the rectorite, corresponds to a total net layer charge of 0·78/unit cell of beidellite, as plotted on Fig. 3. Such a total net layer charge is similar to that of the montmorillonite samples giving 17 — re-expansion. Although the exact amount of the net layer charge of the synthetic beidellites is uncertain, the charge must be predominantly in the tetrahedral sheet because the clays contain no Mg^{2+} or other cation that can give a net charge to the octahedral sheet. The fact that three of the synthetic beidellites re-expand to 17 Å supports the implication from the rectorite that re-expansion after K^+-saturation is not limited by a high proportion of net tetrahedral sheet charge.

Figure 3 clearly indicates that re-expansion of K^+-saturated montmorillonite and probably also beidellite is much more closely related to total net layer charge than to the position of that charge within the layer. However, it should be recognized that other applications of K^+-saturation described in the literature have not generally involved heat treatment as high as 300°C, nor has ethylene glycol been used in all instances to promote re-expansion. Therefore, the results of different investigators are not strictly comparable.

NET LAYER CHARGE OF TYPES OF MONTMORILLONITE

The lines on Fig. 3 at a total net layer charge of 0·85/unit cell and at 15 and 50 per cent of the net charge in the tetrahedral sheet divide the diagram into areas corresponding approximately to different types of montmorillonite. About $\frac{1}{5}$ of the samples have parameters that do not plot in the expected area, but most of these samples either are transitional types or have compositions such that the structural formula is as likely to be incorrect as deviation from the general pattern is likely to be real.

Otay-type samples typically have a large net layer charge that is almost entirely in the octahedral sheet. Exceptions are as follows: (1) Sample no. 44 has an exceptionally small net layer charge of 0·75/unit cell. Its calculated interlayer cations (Table 3) include 0·19 Mg^{2+}/unit cell, but the experimentally determined exchangeable Mg^{2+} is 70 me/100 g of fired material, which corresponds to 0·25 Mg^{2+}/unit cell. The addition of 0·06 Mg^{2+} to interlayer positions raises the total net layer charge to 0·87/unit cell and into the expected area on Fig. 3. (2) Samples no. 35 and no. 43 have calculated net charges in their tetrahedral sheets that are larger than for most Otay-type samples. The Li^+-test indicates a smaller net charge in the tetrahedral sheet for both samples. Also, sample no. 34 is from the same locality as no. 35 (Table 1) but has a much smaller net charge in the tetrahedral sheet (Table 3).

Most Chambers-type montmorillonites have a total net layer charge greater than 0·85/unit cell that is between 15 and 50 per cent in the tetrahedral layer. Exceptions are as follows: (1) The Polkville (E) sample (no. 49) has no calculated net charge in the tetrahedral sheet. However, as discussed in connection with the Li^+-test, this sample apparently is mislabeled. Published data indicate that the original sample actually is Otay-type, and that the Chambers-type symbol rather than the plotted position on Fig. 3 is incorrect. (2) The Shoshone sample (no. 51) has parameters that plot slightly outside the expected area on Fig. 3. A more recent analysis of a sample from this locality (no. 52) plots within the expected area.

Tatatilla-type samples, with one apparent exception, plot in the same area on Fig. 3 as the Chambers-type montmorillonites. The exception is the Rhön(GK) sample (no. 33), which, with 51 per cent of its net layer charge in the tetrahedral sheet, might better have been classed as a beidellite, as other workers have done (Weiss, Koch and Hofmann, 1955, p. 15; Weir, 1965). The plotted position of sample no. 33 thus is not inconsistent. However, it is grouped here with the Tatatilla-type montmorillonites because the high temperature at which it dehydroxylates (Table 3) is atypical of most beidellites, and its net layer charge distribution is just barely in the beidellite range. Also, this classification facilitates comparison with the second Rhön sample (no. 32) which is composed mostly of montmorillonite that is well outside the beidellite range. With the Li^+-test, sample no. 32 gives two 002/004 reflections that indicate a mixture of 80 per cent Tatatilla-type montmorillonite having 25 per cent re-expanding layers and about 20 per cent beidellite that is almost completely re-expanding.

All of the K^+-treated non-ideal montmorillonites re-expand to considerably less than 17 Å, but two of the five samples have calculated net layer charges considerably less than 0·85/unit cell. Woburn sample no. 63, reported by Mackenzie (1960, 1963) to have a charge on its interlayer cations of

https://doi.org/10.1346/CCMN.1969.0170302 Published online by Cambridge University Press

0·70/unit cell, was obtained from the same source as Mackenzie's Woburn sample, although several years later, so that identity is somewhat uncertain. Mackenzie's structural formula has nevertheless been applied to sample no. 63. Woburn sample no. 64 was derived from no. 63 by fractionation and chemical purification. The different MgO contents of no. 63 and no. 64 (Table 2) suggest that Mackenzie's chemical formula perhaps should not be applied to no. 63. Alternately, the 0·10 Al^{3+} that is in excess of the ideal total of 4·00 octahedral cations perhaps should be shown in interlayer positions of the structural formula for sample no. 63. This would increase the calculated net layer charge to an amount more in line with the limited re-expansion of the K^+-treated sample. Incomplete collapse after untreated sample no. 63 is heated at 300°C and its clay–water slurry pH of 6·0 indicates presence of stable gibbsite-like interlayer material before purification. No Al^{3+} was transferred to interlayer positions on Table 3 because Mackenzie's chemical analysis was of Ca^{2+}-saturated clay, but the Ca^{2+}-saturation may not have removed all of the interlayer Al^{3+}. The other non-ideal montmorillonite sample with small layer charge is no. 68 from Redhill (GK), which gives no particular reason for suspecting the structural formula other than the limited re-expansion of the K^+-treated sample itself. This Redhill sample is a mixture of nearly equal amounts of Chambers-type and non-ideal montmorillonite, both of which normally have high net layer charge.

Wyoming-type montmorillonites mostly have a net layer charge less than 0·85/unit cell that is 15–50 per cent in the tetrahedral sheet. The 5 per cent net charge calculated in the tetrahedral sheet of sample no. 19 is not consistent with its Li^+-test, and the exceptionally large corrections for 10 per cent biotite and 10 per cent plagioclase make its structural formula more than normally suspect. In contrast, no such explanation can be applied to sample no. 18, but re-expansion to a spacing of 17+ by sample no. 18 as well as no. 19 after K^+-treatment indicates that the calculated net layer charge is too high for both samples. Two Wyoming-type montmorillonites (nos. 6 and 13) have slightly more than 50 per cent of their net layer charge in the tetrahedral sheet, but their reaction to the Li^+-test suggests that their actual tetrahedral charge is slightly lower than calculated for the Little Rock (E) sample (no. 6) and considerably lower for the Bates Park sample (no. 13). Four other Wyoming-type montmorillonites have net layer charges over 0·85/unit cell (nos. 10, 12, 24 and 27), and all re-expand to less than 17 Å. Two of these were produced from normal Wyoming-type samples (nos. 9 and 11) during the Na^+-citrate-dithionate purification, which reduced $\frac{1}{4}$ to $\frac{1}{2}$ of their Fe^{3+} to Fe^{2+}, thereby increasing the net layer charge beyond the point where they will re-expand to 17 Å after the K^+-treatment. Sample no. 27 seems to be intermediate between Wyoming- and Chambers-type, judged from its net layer charge and DTA characteristics. However, properties of samples nos. 10, 12 and 24, notably their DTA curves, are typical of Wyoming-type samples, indicating that differences other than layer charge must be involved between Wyoming- and Chambers-type montmorillonites.

DIFFERENTIAL THERMAL ANALYSIS

All DTA runs were made in apparatus similar to that described by Grim and Rowland (1942) with a heating rate of about 12°C/min, a galvanometer-photopen recording system, and a nickel block with sample wells $\frac{3}{8}$ in. deep, $\frac{1}{4}$ in. in diameter and holding approximately $\frac{1}{2}$ g of sample. All were run at half of the maximum sensitivity.

DTA curves typical of the different types of montmorillonite are reproduced on Fig. 4. Most samples show the usual interlayer water relationships, with a single endotherm at about 150°C for clays with exchangeable Na^+ (Fig. 4, sample no. 1) and a double endotherm at about 150° and 220°C for clays with exchangeable Ca^{2+} (Fig. 4, sample no. 28). An exception, which gives a pronounced doublet at about 140°C and 190°C (Fig. 4, sample no. 61) will be discussed later. Otherwise, only the dehydroxylation temperature, the shape of curve ending above 800°C, and the firing product will be considered. Most samples were fired to 1000°C, but a few were heated as high as 1100°C to complete their characteristic ending (Fig. 4, no. 28).

Wyoming-type montmorillonites give a dehydroxylation endotherm with the peak at 700–725°C. Their curve endings consist of a weak endotherm near 900°C ± 10°C followed immediately by a moderately strong exotherm about 40°C higher (Fig. 4, no. 1, W-type ending). The spinel firing product reported by Earley, Milne, and McVeagh (1953) for Wyoming-type montmorillonites generally was not found in this study. The only evidence for development of crystalline material from Wyoming-type samples heated to 1000°C is a trace of spinel in samples nos. 22 and 27, both of which contain interlayer Mg^{2+}.

Otay-type samples give dehydroxylation peaks at temperatures from 650° to 690°C, which are consistently lower than those of Wyoming-type samples. The DTA curve ending invariably includes three elements: first a large endothermal peak at 840° ± 20°C, followed by a slight to pronounced shoulder, and finally a broad, weak to moderately strong exotherm between 1000° and

https://doi.org/10.1346/CCMN.1969.0170302 Published online by Cambridge University Press

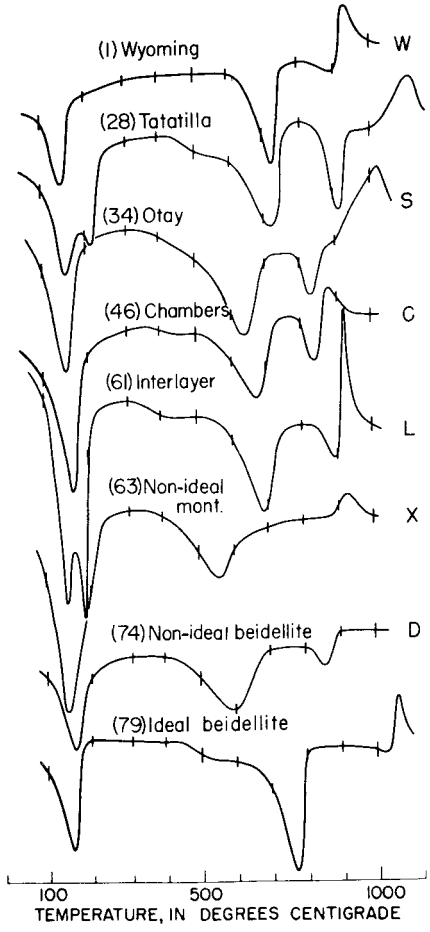


Fig. 4. DTA curves typical of different types of aluminous smectite. Numbers indicate samples used for tracings. Letters at right indicate type of ending listed on Table 3: W—Wyoming; S—shoulder; C—Chambers; L—very large endotherm and exotherm; X—exotherm only; D—endotherm only.

1100°C. Beta-quartz, a high temperature variety containing Al^{3+} and alkali ions (Bradley and Grim, 1951), is the high-temperature phase of all Otay-type samples studied except no. 34 which produced a trace of spinel.

Tatatilla-type montmorillonites give dehydroxylation peak temperatures similar to those of Wyoming-types, 710–730°C. The shape of the DTA curve endings are of either S- or D-type. Those with S-type endings produce mullite and in one sample also a trace of cordierite. Those with D-type endings produce amorphous material.

Chambers-type samples give dehydroxylation peak temperatures at 660–690°C, which are similar to those of Otay-type samples. Most give endings with a strong endotherm at about 850° ± 20°C followed immediately by a moderate to strong exotherm (C-type ending, Fig. 4). The firing product of most samples is amorphous, rarely with a little spinel. Some samples classed as Chambers-type give a somewhat different type of ending, with a strong endotherm at about 910 ± 15°C followed by an exceptionally strong and sharp exotherm about 30°C higher (Fig. 4, sample no. 61, L-type ending). All four samples giving such an ending (nos. 58, 60, 61 and 62) fire to mullite or spinel and also give the unusual low-temperature double endotherm at 140 ± 10°C and 175 ± 15°C illustrated for sample no. 61. Such samples are called "Interlayer" variants of the Chambers-type because the unusual features seem related in some way to presence of stable gibbsite-like interlayer material. Samples nos. 59 and 44, which have abundant interlayer brucite-like material, also give the unusual double endotherms like sample no. 61, but not the L-type endings. It is not clear why other samples with abundant interlayer Al^{3+} or Mg^{2+}, such as sample no. 53, do not also give DTA curves of the interlayer type.

Beidellites and non-ideal montmorillontes have no single characteristic type of DTA ending (Table 3). Beidellite samples with little or no iron give mullite as their high-temperature phase. Others give amorphous material.

The distinguishing feature of the DTA curves of non-ideal montmorillonites is the low dehydroxylation temperature of 560–590°C. All other montmorillonites have their major dehydroxylation peak temperature between 650° and 735°C. The essential correctness of the chemical composition for the non-ideal montmorillonites seems well established by the essential agreement between repeated analyses of the Atzcapozalco sample (nos. 65, 66 and 67) and of the Woburn sample (nos. 63 and 64). Structural formulas calculated from all these analyses are well within the normal compositional range of montmorillonite.

All of the natural beidellites (nos. 69–78, Table 3) give dehydroxylation peak temperatures between 550 and 600°C, which is within the lower range defined earlier in this paper as non-ideal. However, three of the synthetic beidellites (nos. 79, 81 and 83) give dehydroxylation peak temperatures of 720–760°C, which are above the normal dehydroxylation temperature of beidellites. The other two synthetic beidellites (nos. 80 and 82) give two dehydroxylation endotherms, one of which is in the normal temperature range, and the other in the higher range. Although exact compositions of

https://doi.org/10.1346/CCMN.1969.0170302 Published online by Cambridge University Press

the synthetic beidellites are somewhat uncertain. behavior of the samples toward the Li^+-test and the absence in their composition of Mg^{2+} or any other element that can produce a net octahedral charge leave no question about their predominantly net tetrahedral layer charge and their essentially beidellitic composition. Beidellites that retain their structural water to such high temperatures are referred to here as ideal beidellites.

DISCUSSION

Dehydroxylation of beidellite at temperatures lower than those of montmorillonite commonly is thought to result from weak bonds caused by large amounts of tetrahedral Al^{3+} in the structure (Johns and Jonas, 1954; Mumpton and Roy, 1956; Jonas, 1961; Cicel, 1963). Although this explanation accounts for a large majority of samples, non-ideal montmorillonites and ideal beidellites seem to require some additional important factor to explain their dehydroxylation temperatures. R. Greene-Kelly (*in* Mackenzie, 1957, p. 149) has suggested structural defects for non-ideal ("abnormal") montmorillonites, a factor that seems generally consistent with data from this study, at least insofar as defects cause a decrease in the sharpness and intensity of X-ray reflections. Diffraction patterns generally, and specifically the intensities of 020 (Table 3) of all non-ideal montmorillonites are weaker than those of the ideal montmorillonites with only one exception (no. 8). Defects might also account for the low dehydroxylation temperatures of several of the beidellites. However, some non-ideal beidellites appear to be well crystallized (no. 70 and possibly no. 76), so their low dehydroxylation temperatures are apparently not due to structural defects. Furthermore, ideal beidellites dehydroxylate at high temperatures, and therefore abundance of tetrahedral Al^{3+} also cannot be a controlling factor. Something else is needed.

Ames and Sand (1958) report that high net layer charge produces maximum dehydroxylation temperatures for montmorillonites, but the relationship does not seem to hold for the group of samples in this study. Wyoming-type montmorillonites have relatively low net layer charges and high dehydroxylation temperatures whereas the non-ideal beidellites and non-ideal montmorillonites mostly have high net layer charge and low dehydroxylation temperature.

Particle size seems not to affect dehydroxylation temperature either. Bayliss (1965) reports no decrease of dehydroxylation temperature in submicron sizes, and no differences were noted in size fractions made from samples nos. 9,11,36 and 63 of this study. Jonas (1961) reports that in some montmorillonite samples the finer particles actually dehydroxylate at a higher temperature than the coarser ones. He attributes the difference not directly to particle size itself but to the fact that only the most stable crystals can exist as very small particles.

Content of major cations other than tetrahedral Al^{3+}, such as Mg^{2+} or Fe^{3+}, also seems unable to account for a major part of the observed variation in dehydroxylation temperature of montmorillonites and beidellites. Relatively large amounts of Mg^{2+} in Otay- and Chambers-type as compared with amounts in Wyoming-type montmorillonites might suggest that Mg^{2+} can decrease dehydroxylation temperature by a few tens of degrees C. However, the dehydroxylation temperature of some beidellites with low Mg^{2+} is minimal and that of some Tatatilla-types with as much Mg^{2+} as Otay- and Chambers-types is as high as that of Wyoming-types. The characteristic chemical feature of the Tatatilla-types is very low iron content (< 1 per cent), which, together with the low dehydroxylation temperature characteristic of nontronites and many iron-rich beidellites (samples nos. 71–75) might suggest that Fe^{3+} depresses the temperature. However, Wyoming-types characteristically contain moderate amounts of Fe^{3+}, and Sudo and Ota (1952) describe an iron-rich montmorillonite from Japan with a structural formula of $X_{1\cdot16}(Al_{1\cdot52}Fe^{3+}_{1\cdot72}Fe^{2+}_{0\cdot18}Mg_{0\cdot96})(Al_{0\cdot62}Si_{7\cdot38})O_{20}(OH)_4$ that gives a DTA endothermal peak at about 670°C. In contrast, Black Jack beidellite (Table 3, nos. 69, 70), with a peak temperature of 560°C, contains practically no iron. The amounts of the major structural cations involved, Al^{3+}, Mg^{2+}, Fe^{3+} and Si^{4+}, seem to exert an influence on the dehydroxylation temperature of no more than ± 50°C.

Common interlayer cations also exert only a minor influence on dehydroxylation temperature (Mielenz *et al*, 1955; Mumpton and Roy, 1956; Mackenzie and Bishui, 1958). Minor and trace elements in the structure, such as Fe^{2+}, Mn, Li, Zn, Cu, V and Ti, occur in such small amounts that they cannot reasonably be a major factor in loss of structural water by the common montmorillonites. About the only remaining factor susceptible to measurement is structural water, the amount of which is measured by thermal gravimetric analysis.

THERMAL GRAVIMETRIC ANALYSIS

TGA curves of 21 samples (Table 4) were run by F. Simon, all on the same apparatus heating at 5°C per min. Although an effort was made to choose only samples with reliable structural formulas and with little or no impurities or interlayer structures, this was not possible for the more unusual types of clay, and even some of the common

https://doi.org/10.1346/CCMN.1969.0170302 Published online by Cambridge University Press

Table 4. Structural water from TGA

No.	Sample Name	Per cent Beidellitic Characteristics: Structural formula	Li Test	DTA Dehydroxylation peak: Temp. °C	Size cm²	Structural water loss per cent ignited wt.: TGA (Fig. 6)	Ideal 4(OH)	Diff.
				Ideal beidellites (synthetic)				
79	Tem-Pres B-1	100	85	760	10	5·2	5·0	+ 0·1
81	Tem-Pres B-3	100	100	730	2	4·2	5·1	
83	Tem-Pres B-5	100	100	725	3	4·6	5·1	
				Ideal montmorillonites				
28	Tatatilla	19	14	725	12	5·3	5·1	+ 0·2
10	Jenne – 0·25 μ	24	20	725	8	5·0	5·0	0·0
12	Moorcroft (S)0·25 μ	28	12	720	8	5·0	5·0	0·0
1	Clay Spur (E)	38	15	720	8	5·2[2]	5·1	+ 0·1
6	Little Rock (E)	51	37	705	11	5·1[2]	5·0	+ 0·1
41	Santa Rita (E)	2	10	690	10	4·9[2]	5·1	− 0·2
46	Chambers (E)	23	20	675	9	5·0	5·0	0·0
37	Sanders – 0·25 μ	7	15	665	7	5·0	5·1	− 0·1
48	Plymouth (E)	41	33	660	7	5·2[2]	5·0	+ 0·2
34	Otay (E)	4	12	650	11	5·0	5·1	− 0·1
				Non-ideal montmorillonites				
64	Woburn – 0·25 μ	25	24	590	8	4·4	4·9	− 0·5
64	Woburn-repeated	25	24	590	8	4·3	4·9	− 0·6
66	Atzcapozalco[1]	27	32	590	11	5·3	5·0	+ 0·3
				Non-ideal beidellites				
74	P-10[1]	56	55	590	9	6·3[2]	4·9	+ 1·4
75	Cameron (W)	50	55	585	8	5·3[2]	4·9	+ 0·4
73	JH-10	66	89	580	7	5·7[2]	4·9	+ 0·8
69	Black Jack[1]	100	100	560	7	6·2	5·1	+ 1·1
71	Beidell	71	60	550	8	8·8	4·9	+ 3·9

[1]50 mg sample; all others 100 mg.
[2]Includes correction for impurities listed in Table 2.

types contain small amounts of quartz or cristobalite. Three of the beidellites (nos. 71, 74 and 75) have considerable interlayer illite, two samples have considerable interlayer brucite-like structures (nos. 66 and 71), and some of the synthetic beidellites have proven to have unreliable structural formulas. The Woburn sample (no. 64) was repeated a second time to give a total of three water analyses for non-ideal montmorillonite.

The TGA curve on Fig. 5 for sample no. 34 is typical of all of the samples run except two of the synthetic beidellites illustrated by sample no. 83. The typical curves all have four distinct segments: (1) an initial rapid loss of interlayer water at about 100°C; (2) a gradually sloping mid-temperature plateau up to 450–600°C; (3) a rapid water loss corresponding to the major dehydroxylation of the structure; and (4) a gradually sloping high-temperature plateau between about 700 and 1000°C. A straight line can be drawn through most of the points on the mid-temperature plateau.

The slope of the mid-temperature plateau indicates that not all adsorbed or interlayer water is lost by montmorillonites before the loss of structural water begins. The problem in the interpretation of the TGA curve is to select a dividing temperature where the amount of unvolatilized interlayer water equals the amount of structural water already lost. There is no general agreement on what this temperature is, and in fact, the temperature almost certainly would depend on the rate of heating and other experimental conditions. Several points were tested on the TGA curves of the ideal montmorillonites to see which corresponded to a loss of an ideal 4(OH) per unit cell. The ideal montmorillonites seemed most likely to contain the

https://doi.org/10.1346/CCMN.1969.0170302 Published online by Cambridge University Press

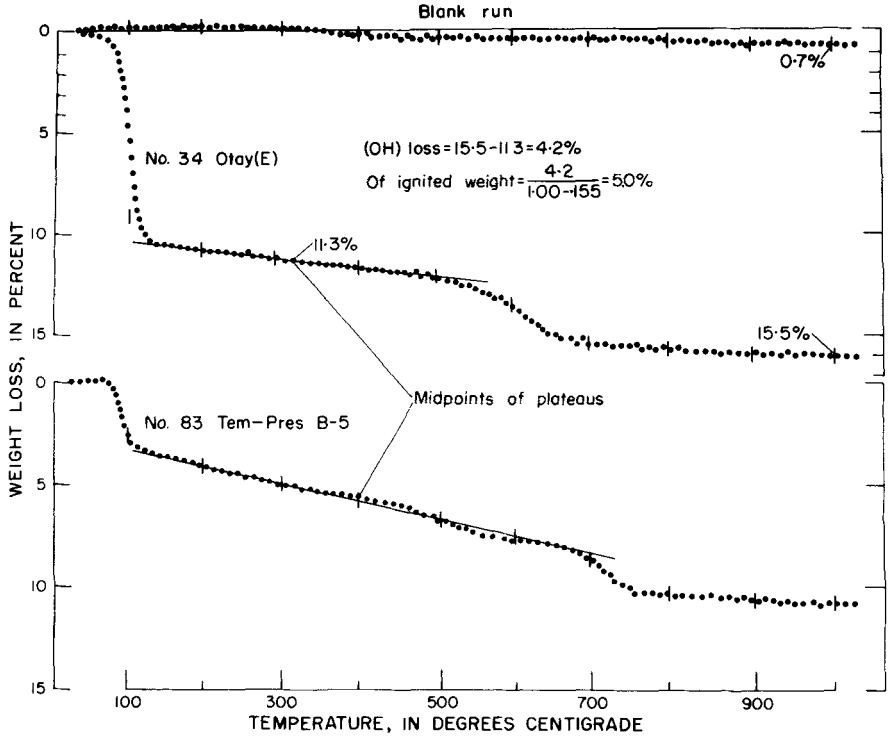


Fig. 5. TGA curves. 5°C/min. Weight loss figures include corrections from blank curve.

ideal amount. The weight loss above 300°C used by Ross and Hendricks (1945, pp. 49–51) and by Weir and Greene-Kelly (1962, p. 142) probably is as good a temperature as there is for slow heating rates (about 100°C/day), but at the heating rate of 5°C/min used for this study, 300°C gives high-temperature water losses for ideal montmorillonites that average 0·2 per cent and are as much as 0·6 per cent more than ideal. The dividing point that most consistently gives high-temperature water losses near the ideal amount for the ideal montmorillonites is the middle of the mid-temperature plateau, the limits of the plateau being defined by the point at each end where the straight line departs from the TGA curve (Fig. 5).

The top curve on Fig. 5 is a blank run made to determine corrections for buoyancy and convection currents for the apparatus used. Heating the air in the furnace decreases its density and its buoyant effect on the inert sample and holder, so that the weight of the sample and holder apparently increases and the curve initially trends slightly upward. Opposing convection currents in the heating chamber exactly counterbalance decreased buoyancy at 350°C, bringing the curve back to its starting point. At 1000°C the dominant convection currents cause an overall apparent weight loss of 0·7 mg.

The structural water content of sample no. 34 is determined as follows (Fig. 5). The apparent weight loss at 1000°C of 16·2 per cent, when corrected for buoyancy effects amounting to 0·7 per cent, becomes a weight loss of 15·5 per cent. The apparent weight loss at the mid-plateau temperature of 330°C of 11·25 per cent, when increased by a correction of 0·05 per cent, becomes 11·3 per cent. The difference in the corrected weight losses gives a high-temperature weight loss of 4·2 per cent of the air-dried sample, which is assumed to be the structural water. This is changed to an ignited weight basis of 5·0 per cent by dividing the 4·2 by the proportion of sample remaining at 1000°C. Structural water values so derived are listed in Table 4 in order of decreasing dehydroxylation temperature of the samples. Also listed are data on the beidellitic character, the size of the DTA dehydroxylation endotherm, and the amount of structural water equivalent to the ideal 4(OH) for each sample.

Two of the TGA curves of synthetic beidellite (nos. 81 and 83) differ from the others. As illustrated on Fig. 5 for sample no. 83, they have exceptionally steep mid-temperature plateaus that

https://doi.org/10.1346/CCMN.1969.0170302 Published online by Cambridge University Press

depart considerably from a straight line, followed by a weak dehydroxylation slope at a very high temperature. In conjunction with the weak X-ray patterns of both samples relative to the other three synthetic beidellites (Table 3) and in conjunction with the small dehydroxylation endotherms (Table 4), such TGA curves are interpreted to indicate a mixture of hydrous amorphous material and a very well crystallized beidellite. The values for structural water on Table 4 for samples 81 and 83 are therefore invalid and are not considered further.

Deviations from ideal structural water contents for the ten ideal montmorillonites and the one reliable ideal beidellite (no. 79) range from +0·2 to −0·2 per cent (Table 4). Points on the TGA curves can be measured to about ±0·1 per cent. Thus, if measuring errors at the top and the bottom of the structural (OH) range were in opposite directions, the cumulative measuring error could account for the deviations from ideal 4(OH) water for the ideal montmorillonites.

Samples with dehydroxylation peak temperatures below 600°C all give amounts of structural water measured above the middle of the mid-temperature plateau that differ from ideal 4(OH) by amounts greater than can be accounted for by measuring errors. The non-ideal beidellites have an excess, and, for all but the Cameron sample, the excess is considerable. The very great excess of high-temperature water measured for the Beidell, Colorado, sample evidently is due not only to extra structural water but also to the abundant and very stable interlayer hydrated structures it contains (Table 3, no. 71). Data for the non-ideal montmorillonites are scant and mixed, but they suggest more a deficiency than an excess of structural water. The small excess of high-temperature water measured for the Atzcapozalco sample may, like that of the Beidell sample, be due to its interlayer hydrated structures. Thus, the presence of structural water in quantities greater than, and possibly also less than, the ideal amount appears to be the major factor controlling dehydroxylation temperature.

DISCUSSION

The importance of structural water to dehydroxylation temperature is also suggested by some data in the literature. Weir and Greene-Kelly (1962, p. 142) report a 5·9 per cent water loss between 300 and 950°C for Black Jack beidellite using very slow heating. (Temperature was raised 50°C every 12 hr; the 6·3 per cent figure given on their page 142 is a printing error and should refer to ignition loss above 105°C according to A. H. Weir (oral commun. (1966).) This indicates an excess of about 0·8 per cent structural water which is in essential agreement with 1·1 per cent measured for the Black Jack sample in this study. Ross and Hendricks' (1945, pp. 49–50) illustrations of Nuttig's TGA curves show montmorillonite samples with water loss above 300°C as follows: Belle Fourche, 4·9%; Otay, 5·1%; Tatatilla, 5·1% Polkville, 5·2%. All four are within a few tenths of a per cent of the ideal structural water, and all give dehydroxylation endotherms near 700°C. The author has not worked with and is unaware of X-ray or DTA data for the Mexico, Irish Creek, and Mainburg samples. Ross and Hendricks' TGA of the Montmorillon sample gives a 5·7% water loss above 300°C, which is 0·7 per cent in excess of ideal; however, judged from the excess of structural water and from the double high-temperature inflection in its TGA curve and its double dehydroxy endotherms (Grim and Kulbicki, 1961, p. 1339, sample 31), this type montmorillonite sample is a mixture of an ideal montmorillonite and a non-ideal beidellite. Ross and Hendricks' two samples with the greatest water loss above 300°C, from Pontotoc and Wagon Wheel Gap, are mostly or entirely non-ideal beidellites, though the exceptionally high losses of 8·5 and 7·5 per cent probably are not entirely due to excess structural water, but are due in part to kaolinite impurity in the former and interlayer gibbsite-like material in the latter (see samples no. 72 and no. 78, Tables 2 and 3, this report). Higashi and Aomine (1962) report amounts of high-temperature water in soil montmorillonites giving DTA dehydroxylation endotherms near 550°C that are markedly higher than that in a Wyoming-type montmorillonite. Mielenz, Schieltz and King (1954, p. 306) illustrate TGA curves run at 5°C/min, that, when interpreted as illustrated on Fig. 5, give 5·2 per cent structural water for an Upton, Wyoming, montmorillonite and 5·3 per cent for an Otay, California, montmorillonite – values that are within about 0·2 per cent of ideal. Their curve for a Belle Fourche sample, however, gives 5·6 per cent structural water above the middle of the mid-range plateau.

Structural water differing in amount from 4(OH) per unit cell may also be an important factor controlling dehydroxylation of other clay minerals. Illite characteristically gives DTA endotherms with peaks in the same 500–600°C range common for beidellite and those of nontronite commonly are in a range that is about 50°C lower. Excess high-temperature water is one of the properties originally listed by Grim, Bray, and Bradley (1937) as characteristic of illite. Mielenz, Schieltz, and King (1954) illustrate TGA curves that, if interpreted in the same way as for montmorillonite in this paper, indicate high-temperature water contents that are 1·8 per cent more than ideal for Fithian illite and 0·7 per cent more than ideal for

https://doi.org/10.1346/CCMN.1969.0170302 Published online by Cambridge University Press

Manito nontronite. The TGA curves illustrated by Ross and Hendricks (1945, p. 51) for three nontronites indicate water loss above 300°C close to the ideal 4(OH), but appreciable structural (OH) might be lost from nontronites when heated at 300°C for as long as their 24 hr heating period.

POSITION OF STRUCTURAL WATER

The Ross and Hendricks (1945) method for computation of structural formulas is based on the Hofmann, Endell and Wilm (1933) structure of montmorillonite (Fig. 6a) in which (OH) occupies anion positions in the octahedral sheet that are not occupied by the apical oxygens of the tetrahedral sheet—e.g., (OH) occurs inside all of the holes formed by the silica rings. As non-ideal montmorillonites seem to contain less than the ideal amount of structural water, some of these (OH) positions must be occupied by oxygen. On the other hand, structural (OH) in non-ideal beidellites in excess of the ideal amount must occur in positions other than inside the silica rings. Several possible positions are illustrated in Fig. 6b–d.

The effect of extra structural (OH) on the calculated structural formula also is shown in Fig. 6. The formula in Fig. 6a is calculated in the conventional way for the Black Jack sample by assuming a total of +44 charges necessary to balance the $[O_{20}(OH)_4]^{-44}$ framework of the structure. If the amount of structural water is not ideal, the calculation must be made on the basis of $[O_{24}]^{-48}$ per unit cell, and the H^+ of the structural water must be included with the balancing cations. The formula in Fig. 6b results from such a calculation using the amount of 6·2% structural water measured from the TGA curve (not illustrated) of the Black Jack sample. The extra H^+ ions cause the calculated amounts of all other cations to decrease. The resulting total of octahedral cations is considerably below the ideal total of 4·00 per unit cell, implying

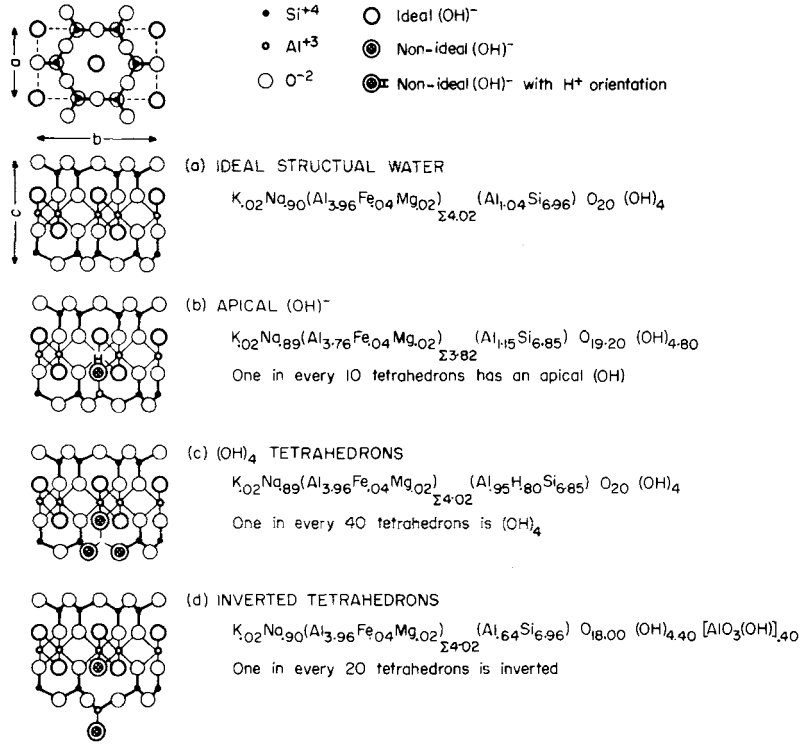


Fig. 6. Possible locations of excess water in beidellite. Schematic structures are adapted from Bragg (1937, p. 206) and in (a) represent the Hofmann, Endell and Wilm (1933) structure of montmorillonite. The a–b plane shows the hexagonal network of silicon-oxygen tetrahedral groups with hydroxyl at the center of each ring. The b–c plane shows two such silica sheets edgewise with apical oxygens sharing positions in the medial sheet of alumina octahedrons. (c) illustrates concepts of McConnell (1951) and (d) of Edelman and Favejee (1940). Structural formulas for the configurations are derived from data for the Black Jack sample (no. 69, Tables 3 and 4).

https://doi.org/10.1346/CCMN.1969.0170302 Published online by Cambridge University Press

that some octahedral cation sites normally occupied are vacant. In Fig. 6b, the extra (OH) is figured in the position shown in order partly to compensate for charge imbalance caused by the vacant octahedral cation site and by the Al^{3+}-for-Si^{4+} substitution, but this is not an essential factor in most of the following discussion.

Occurrence of structural water in tetrahedral positions as suggested by McConnell (1951) is illustrated in Fig. 6c. Four H^+ ions are assumed to replace one Si^{4+} in the structural formula, and the number of octahedral cations thus remains close to the ideal 4·00 per unit cell.

Inverted tetrahedrons (Fig. 6d), first suggested by Edelman and Favejee (1940), have one (OH) at the tip of the inverted tetrahedron and a second extra (OH) in the otherwise vacant anion site left by the inversion. Thus, each inversion substitutes two $(OH)^-$ for one O^{2-} of the ideal structure, which amounts to the addition of an uncharged H_2O molecule, and the distribution of other cations is essentially the same as that implied by the Ross and Hendricks (1945) formula.

An attempt is made in the following section to determine in which of the positions illustrated in Fig. 6 the extra structural water of beidellite actually occurs.

HEATING X-RAY DIFFRACTOMETRY

The structure factor (F) for 00*l* reflections is equal to $\Sigma_j f_j \cos 2\pi l z_j$, where f_j is the atomic scattering factor of the j^{th} atom, l is the Miller index, and z_j is the z-coordinate of the j^{th} atom. Thus, mass lost from different Z levels in a structure effects (F) differently. Inasmuch as intensity (I) is proportional to $(F)^2$, some discrimination between the different occurrences of extra structural water might be possible from observation of changes in X-ray intensities when a sample is heated through its dehydroxylation range.

Changes in $(F)^2$ for the first three basal reflections of the Black Jack beidellite (no. 69) calculated first for loss of ideal structural water, and then for loss of the measured 0·8 extra structural (OH) per unit cell from different positions are as follows:

The increase or decrease in I_{00l} also can be inferred from the graphic presentation on Fig. 7. As an example, for the 001 reflection, the position of ideal (OH) corresponds to 42° ($2\pi lz$), the cosine of which is large and positive, so loss of this (OH) should cause a large decrease in F_{001} and consequently in I_{001}. For the 002 the cosine is very slightly negative, so loss of ideal (OH) should cause a slight increase in I_{002}. For the 003 the cosine is negative and fairly large, so loss of ideal (OH) should cause a considerable increase in I_{003}.

Extra structural water lost from apical positions of silica tetrahedrons (Fig. 6b) will have the same effect on I_{00l} as loss of ideal (OH) because both would be lost from the same Z level, but the change would be less because much less extra water is involved.

The changes in I_{00l} for $(OH)_4$ tetrahedrons (Fig. 6c) and inverted tetrahedrons (Fig. 6d) are calculated assuming that the oxygen of the volatilized water comes from the outer oxygen plane of the structure. For the $(OH)_4$ tetrahedron, three-fourths

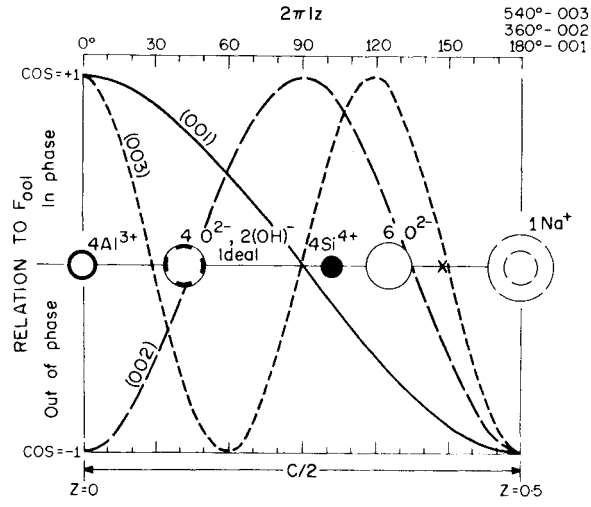


Fig. 7. Angular relations for $F_{00l} = \Sigma_j f_j 2\pi l z_j$ of smectite along [001]. X indicates position of Si^{4+} or Al^{3+} of inverted tetrahedron outside the layer.

	Change in $(F)^2$ due to (OH) loss		
	001 (%)	002 (%)	003 (%)
Ideal 4(OH) – Fig. 6a	− 64	+ 7	+ 17
Apical (OH) – Fig. 6b	− 15	+ 1	+ 3
(OH) from outside plane-Figs. 6c, 6d	+ 10	− 3	− 4
Shift of inverted Si^{4+} or Al^{3+}	+ 20	+ 27	+ 4

https://doi.org/10.1346/CCMN.1969.0170302 Published online by Cambridge University Press

of the extra (OH) are in this outer plane, and these should be lost more readily than oxygen of the apical (OH) from inside the structure. The apical (OH) at the tip of the inverted tetrahedron (Fig. 6d) would have to fit into the hole in the silica ring of the adjacent layer when the clay is heated in order for the 001 *d*-value to decrease to the observed 9·6 Å. Thus, the apical (OH) would be essentially in the outer oxygen plane of the adjacent layer, and its loss during dehydroxylation would have the same effect on I_{001} as loss of water from $(OH)_4$ tetrahedrons. However, in the case of the inverted tetrahedron, when the (OH) is lost the Si^{4+} or Al^{3+} probably would shift from its position outside the layer, indicated by "X" on Fig. 7, to its normal positions within the layer. The resulting additional changes in intensity would augment the change in I_{001} due to (OH) loss and would counteract the changes in I_{002} and I_{003}.

Because of uncertainty of changes in I_{002} and I_{003} due to possible shifts in position of Si^{4+} or Al^{3+} of inverted tetrahedrons, attention is focused on I_{001}. As shown above, loss of 0·8 extra (OH) per unit cell from any of the structural positions considered should cause a change in I_{001} of at least 10 per cent. Such a change should be easily observed, provided that the extra water is lost measurably before the ideal water. This seems particularly likely for the $(OH)_4$ tetrahedron or for the inverted tetrahedron configuration, because the extra (OH) is lost from the outer planes of the layer. Also, these two configurations should cause a reversal in intensity change, with an initial I_{001} increase during loss of extra water, followed by an I_{001} decrease during loss of ideal water. Such a reversal should be easier to detect than the continuous decrease expected from loss of the extra apical (OH) inside the layer followed by loss of ideal (OH) from the same structural plane.

The sample actually used for the heating X-ray diffractometer test was P-10 (no. 74) because it contained a large amount of extra structural water (Table 4), and because no additional Black Jack material was available for the test. The sample was stabilized in the heating diffractometer at 200°C for 24 min and then the temperature was raised at the rate of 5°C/min. The trace (Fig. 8) was run at a speed of 2°/min oscillating between 8° and 10°2θ, so that a scan back and forth across the 001 peak was made every 2 min at 10°C temperature intervals. The averages of the increasing and decreasing 2θ scans are marked by the heavy short horizontal lines. There is no suggestion of a rise in intensity near 400–500°C where structural water is first lost. Thus, the heating test seems to place the excess water of beidellites not in $(OH)_4$ or inverted tetrahedrons, but rather in apical positions of normally oriented tetrahedrons. The most critical assumption made in reaching this conclusion is that (OH) in the outer planes of the beidellite layer would leave the structure measurably before those from the inner planes of the octahedral sheet of the layer. Otherwise, the effect on intensity of the much more abundant ideal (OH) lost from inside the structure would overwhelm the opposite effect on intensity of any (OH) lost from outer oxygen planes.

The apical tetrahedral location of excess (OH)

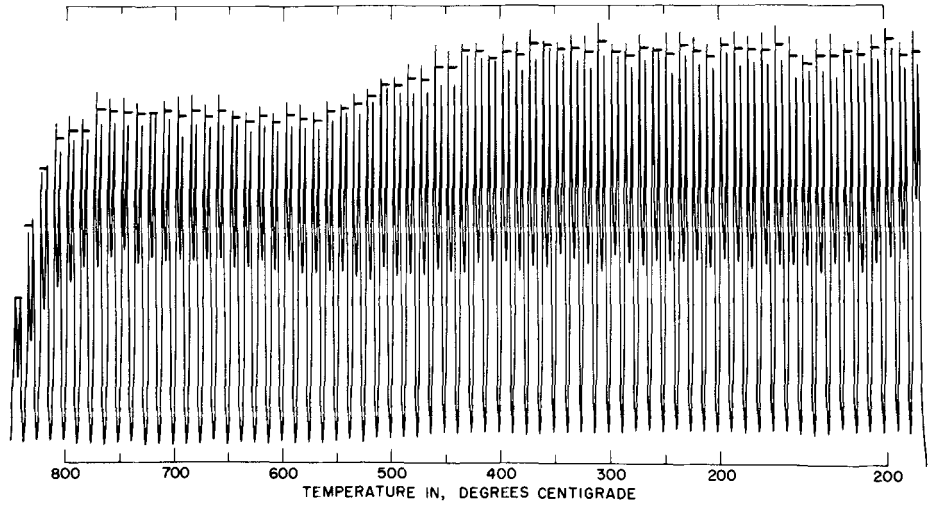


Fig. 8. Diffractometer trace oscillating across the 001 of beidellite sample no. 74 during dehydroxylation.

https://doi.org/10.1346/CCMN.1969.0170302 Published online by Cambridge University Press

indicated by the heating diffractometer experiment requires some further explanation from the standpoint of charge location. Association of the extra $(OH)^-$ with tetrahedral Al^{3+} (Fig. 6b) might seem to decrease the net tetrahedral charge. At the same time the octahedral cation deficiency would cause net octahedral charge that should be neutralized in the Greene–Kelly test by Li^+ ions entering the vacant octahedral holes, thereby decreasing the expansibility of the clay. This does not occur. Expansibility of Black Jack beidellite, for example, is just as complete after the Li^+-treatment as before. Thus, an additional assumption must be made in an attempt to reconcile the water data with the Li^+-test. The assumption is that the H^+ ions of the extra apical $(OH)^-$ point inward toward the octahedral hole and away from the tetrahedral Al^{3+} (Fig. 6), thereby compensating for the positive charge deficiency caused by vacancies in the octahedral sheet but not the charge deficiency caused by Al^{3+}-for-Si^{4+} substitution that is characteristic of beidellites.

Structural water in diverse positions in the beidellite structure might be expected to absorb infrared (i.r.) radiation differently. Attempts to resolve different (OH) absorption wavelengths by using KBr pellets in an i.r. heating stage at 300°C, or by heating clay films in vacuum at 100°C and then protecting from atmospheric water with Nujol mineral oil have not been successful. Possibly the techniques and apparatus were not sufficiently refined. Farmer and Russell (1964, p. 1153 and Fig. 2) report dual absorption bands due to (OH) stretching vibrations in Black Jack beidellite, but they ascribe the second absorption to the effect of Al^{3+}-for-Si^{4+} substitution on normal structural (OH).

SUMMARY

Many features characteristic of the different types of montmorillonite are summarized on Table 5. General conclusions from this study are:

(1) The Greene–Kelly Li^+-test discriminates between beidellites and montmorillonites. If impurities prevent use of the conventional method for estimation of the proportion of re-expanding beidellite-like layers, then the relative intensities of the 9·6 Å and 18 Å reflections before and after glycerol treatment can be used as an approximate auxiliary method.

(2) K^+-saturation, heating to 300°C for ½ hr, and the degree of re-expansion after ethylene glycol treatment are related to the total net layer charge of Al smectites. Wyoming-type montmorillonites have low net layer charge and re-expand to 17 Å. Other types of montmorillonite have high net layer charge and re-expand to 13–16 Å. The same relationship of net layer charge to re-expansion seems to be true for beidellites, but the limited number of samples and relatively uncertain layer charge calculations for some samples make this interpretation less certain.

(3) The net layer charge can be changed by oxidation or reduction of iron in the structure.

(4) TGA curves indicate an amount of structural water in ideal montmorillonites corresponding almost exactly to the ideal amount of 4(OH) per unit cell, provided that this water loss is measured between the mid-point of the mid-temperature plateau and 1000°C. The ideal beidellite, which has a high dehydroxylation temperature similar to that of ideal montmorillonite, also contains an ideal $4(OH)^-$ per unit cell.

(5) The low dehydroxylation temperatures of non-ideal montmorillonites may result from their less-than-ideal amounts of structural water, but may also be due to structural defects.

(6) Non-ideal beidellites contain more than the ideal amount of structural water. The extra water

Table 5. Characteristic features of types of aluminous smectite

Type		Net negative layer charge		DTA				TGA
		Amount	Location	MgO (%)	Fe_2O_3 (%)	Dehydroxylation temp. (°C)	Ending (Fig. 4)	Structural (OH)
Ideal Montmorillonites	Wyoming	low	oct. > tet.	2–3	3–4	700–725	W	= 4
	Tatatilla	high	oct. > tet.	2–4	< 1	700–735	variable	= 4
	Otay	high	oct. ≥ tet.	3½–5	1–2	650–690	S	= 4
	Chambers	high	oct. > tet.	3–4½	1–4	660–690	C	= 4
Non-ideal beidellite		mostly high	oct. < tet.	0–2	0–8	550–600	variable	> 4
Ideal beidellite		variable	tet.	0	0	720–760	variable	= 4
Non-ideal montmorillonite		mostly high	oct. > tet.	2–4	5–10	550–590	variable	< 4?

https://doi.org/10.1346/CCMN.1969.0170302 Published online by Cambridge University Press

seems to be the only possible major cause of their low dehydroxylation temperatures.

(7) The extra water of non-ideal beidellites appears to be located in the structure at the apical corners of tetrahedrons, with the H^+ polarized toward vacancies in the octahedral layer. However, questionable assumptions may have been made in arriving at this conclusion.

(8) Amounts of structural water other than the ideal 4(OH) per unit cell may also have a controlling influence on the dehydroxylation temperature of other layer silicates, such as illite and nontrite.

(9) The sum of Mg^{2+} and Fe^{3+}, but not necessarily either by itself, may have an effect of perhaps $\pm 50°C$ on the dehydroxylation temperature of ideal montmorillonite. Large amounts of octahedral Mg^{2+} might cause the lower dehydroxylation temperature of Otay- and Chambers-types relative to Wyoming-type, but equally large amounts in some Tatatilla-type samples do not produce the same effect. The high dehydroxylation temperature of Tatatilla-type samples might be related to low Fe^{3+} content, except that a few other samples with similarly low Fe^{3+} content lose their structural water at notably lower temperatures. However, most samples with a total content of Mg^{2+} and Fe^{3+} oxides greater than about 6–7 per cent give dehydroxylation peak temperatures below 700°C.

(10) Tetrahedral Al^{3+} commonly, but not always, is accompanied by extra structural water, and therefore is related only indirectly to temperature of dehydroxylation.

(11) Thermal reactions at the ends of DTA curves and firing products are characteristic only for some types of montmorillonite. The Otay-type samples give a shoulder between the concluding endotherm and exotherm, and most of them fire to beta quartz. Some Tatatilla-type samples give a similar shoulder-type ending, but fire to mullite. The curves of Wyoming- and Chambers-type samples are similar in that the exotherm immediately follows the endotherm without a shoulder, but the endotherm of the Wyoming-type is much weaker. Both fire mostly to amorphous material. A variant of the Chambers-type gives an exceptionally large and sharp concluding exotherm, fires to mullite and/or spinel, and commonly also gives an unusual beginning endotherm doublet between 100 and 200°C that apparently is related to abundant gibbsite-like interlayer material.

REFERENCES

Ames, L. L., Jr., and Sand, L. B. (1958) Factors effecting maximum hydrothermal stability in montmorillonites: *Am. Mineralogist* **43**, 641–48.

Anderson, D. M., and Reynolds, R. C. (1966) Umiat bentonite–An unusual montmorillonite from Umiat, Alaska: *Am. Mineralogist* **51**, 1443–56.

Barshad, I. (1954) Cation exchange in micaceous minerals–[Pt.] II, Replaceability of ammonium and potassium from vermiculite, biotite, and montmorillonite: *Soil Sci.* **78**, 57–76.

Bayliss, P. (1965) Differential thermal analysis; Effect of particle size: *Nature, Lond.* **207**, 284.

Brackett, R. N., and Williams, J. F. (1891) Newtonite and rectorite–two new minerals of the Kaolinite Group: *Am. J. Sci.* **42**, 11–21.

Bradley, W. F. (1950) The alternating layer sequence of rectorite: *Am. Mineralogist* **35**, 590–95.

Bradley, W. F., and Grim, R. E. (1951) High temperature thermal effects of clay and related minerals: *Am. Mineralogist* **36**, 182–201.

Bragg, W. L. (1937) *Atomic Structure of Minerals*: Cornell Univ. Press, New York 292 pp.

Brown, G. (Editor) (1961) *The X-ray Identification and Crystal Structures of Clay Minerals*, 2nd End: Mineralogical Soc. (Clay Minerals Group), London, 544 pp.

Brown, G. and Weir, A. H. (1963) The identity of rectorite and allevardite: *Proc. Intern. Clay Conf., Stockholm*, Pergamon Press, New York, 27–35.

Cicel, B. (1963) On the problem of bond strength of OH group in layer silicates: *Geol. Práce, Zprávy* **30**, 249–68.

Earley, J. W., Milne, I. H., and McVeagh, W. J. (1953) Thermal dehydration and X-ray studies on montmorillonite: *Am. Mineralogist* **38**, 770–83.

Earley, J. W., Osthaus, B. B., and Milne, I. H. (1953) Purification and properties of montmorillonite: *Am. Mineralogist* **38**, 707–24.

Edelman, C. H., and Favejee, J. Ch. L. (1940) On the crystal structure of montmorillonite and halloysite: *Z. Krist.* **102**, 417–31.

Farmer, V. C., and Russell, J. D. (1964) The i.r. spectra of layer silicates: *Spectrochim. Acta* **20**, 1149–73.

Ferguson, H. G. (1921) The limestone ores of Manhatten, Nevada: *Econ. Geol.* **16**, 1–36.

Fournier, R. O. (1965) Montmorillonite pseudomorphic after plagioclase in a prophyry copper deposit: *Am. Mineralogist* **50**, 771–77.

Greene-Kelly, R. (1955) Dehydration of the montmorillonite minerals: *Mineral. Mag.* **30**, 604–15.

Grim, R. E., Bray, R. H., and Bradley, W. F. (1937) The mica in argillaceous sediments: *Am. Mineralogist* **22**, 813–29.

Grim, R. E., and Kulbicki, G. (1961) Montmorillonite–High temperature reactions and classification: *Am. Mineralogist* **46**, 1329–69.

Grim, R. E., and Rowland, R. A. (1942) Differential thermal analysis of clay minerals and other hydrous materials, Pts. 1 and 2: *Am. Mineralogist* **27**, 746–61, 801–18.

Harward, M. E., and Brindley, G. W. (1965) Swelling properties of synthetic smectites in relation to lattice substitutions: *Clays and Clay Minerals* **13**, 209–22. [Pergamon Press, New York].

Heide, F. (1928) Beiträge zur Mineralogie und Petrographie der Rhön: *Chem. Erde* **3**, 91–7.

Heystek, H. (1963) Hydrothermal rhyolitic alteration in the Castle Mountains, California: *Clays and Clay Minerals* **11**, 158–68. [Pergamon Press, New York].

Higashi, T., and Aomine, S. (1962) Weathering of montmorillonite in soils: *Soil Sci. Plant Nutr.* **8**, 7–12.

https://doi.org/10.1346/CCMN.1969.0170302 Published online by Cambridge University Press

Hofmann, U., Endell, K., and Wilm, D. (1933) Kristallstruktur und Quellung von Montmorillonit: *Z. Krist.* **86**, 340–8.

Jackson, M. L. (1958) *Soil chemical analysis:* Prentice-Hall, Englewood Cliffs, N.J., 498 pp.

Johns, W. D., and Jonas, E. C. (1954) Some observations on the relation between isomorphism and properties of clays: *J. Geol.* **62**, 163–71.

Jonas, E. C. (1961) Mineralogy of the micaceous clay minerals: *21st Intern. Geol. Congr. Copenhagen 1960, Rept.*, pt. 2, 7–16.

Kelley, W. P. (1955) Interpretation of chemical analyses of clays: *Clays and Clay Tech.* **1**, 92–4. [Calif. Div. Mines Bull. **169**].

Kerns, R. L., Jr., and Mankin, C. J. (1968) Structural charge site influence on the interlayer hydration of expandable three-sheet clay minerals: *Clays and Clay Minerals* **16**, 73–81.

Kerr, P. F. (1932) Montmorillonite or smectite as constituents of fuller's earth and bentonite: *Am. Mineralogist* **17**, 192–8.

Kerr, P. F., Hamilton, P. K., and Pill, R. J. (1950) Analytical data on reference clay minerals: *Am. Petrol. Inst. Project 49, Clay Mineral Standards, Prelim. Rept. 7*, 160 pp.

Kerr, P. F., Kulp, J. L., and Hamilton, P. K. (1949) Differential thermal analyses of reference clay mineral specimens: *Am. Petrol. Inst. Project 49, Clay Mineral Standards, Prelim. Rept. 3*, 48 pp.

Kodama, H. (1966) The nature of the component layers of rectorite: *Am. Mineralogist* **51**, 1035–55.

Koizumi, M., and Roy, R. (1959) Synthetic montmorillonoids with variable exchange capacity: *Am. Mineralogist* **44**, 788–805.

Mackenzie, R. C. (Editor) (1957) *The differential thermal investigation of clays*: Mineralogical Soc. (Clay Minerals Group), London, 456 pp.

Mackenzie, R. C. (1960) Evaluation of clay-mineral composition with particular reference to smectites: *Silicates Ind.* **25**, 12–18, 71–5.

Mackenzie, R. C. (1963) Retention of exchangeable ions by montmorillonite: *Proc. Intern. Clay Conf., Stockholm*. Pergamon Press, New York, 183–93.

Mackenzie, R. C., and Bishui, B. M. (1958) The montmorillonite differential thermal curve—II, Effect of exchangeable cations on the dehydroxylation of normal montmorillonite: *Clay Minerals Bull.* **3**, 276–86.

McConnell, D. (1951) The crystal chemistry of montmorillonite—II. Calculation of the structural formula: *Clay Minerals Bull.* **1**, 179–88.

Melhase, J. (1926) Mining bentonite in California: *Eng. Mining J.* **121**, 837–42.

Mielenz, R. C., Schieltz, N. C., and King, M. E. (1954) Thermogravimetric analysis of clay and clay-like minerals; *Clays and Clay Minerals* **2**, 285–314. [*Nat. Acad. Sci.-Nat. Res. Council Publ.* **327**].

Mielenz, R. C., Schieltz, N. C., and King, M. E. (1955) Effect of exchangeable cation on X-ray diffraction patterns and thermal behavior of a montmorillonite clay: *Clays and Clay Minerals* **3**, 146–73, [*Nat. Acad. Sci.-Nat Res. Council Publ.* **395**].

Mumpton, F. A., and Roy, R. (1956) The influence of ionic substitution on the hydrothermal stability of montmorillonoids: *Clays and Clay Minerals* **4**, 337–9. [*Nat. Acad. Sci.-Nat. Res. Council Publ.* **456**].

Nagelschmidt, G. (1938) On the atomic arrangement and variability of the members of the montmorillonite group: *Mineral. Mag.* **25**, 140–55.

Ross, C. S., and Hendricks, S. B. (1945) Minerals of the montmorillonite group, their origin and relation to soils and clays: *U.S. Geol. Surv. Prof. Paper* **205-B**, 23–79 [1946].

Ross, C. S., and Shannon, E. V. (1926) The minerals of bentonite and related clays and their physical properties: *J. Am. Ceram. Soc.* **9**, 77–96.

Ross, C. S., and Stephenson, L. W. (1939) Calcareous shells replaced by beidellite: *Am. Mineralogist* **24**, 393–7.

Schultz, L. G. (1963) Clay minerals in Triassic rocks of the Colorado Plateau: *U.S. Geol. Surv. Bull.* **1147-C**, CI-C71.

Schultz, L. G. (1966) Lithium and potassium absorption, differential thermal, and infrared properties of some montmorillonites (abs.): *Clays and Clay Minerals* **13**, 275. [Pergamon Press, New York].

Sudo, T., and Ota, S. (1952) An iron-rich variety of montmorillonite found in "Oya-ishi": *J. Geol. Soc. Japan* **58**, 487–91.

Wear, J. I., and White, J. L. (1951) Potassium fixation in clay minerals as related to crystal structure: *Soil Sci.* **71**, 1–14.

Weaver, C. E. (1958) The effects and geologic significance of potassium "fixation" by expandable clay minerals derived from muscovite, biotite, chlorite, and volcanic material: *Am. Mineralogist.* **43**, 839–61.

Weir, A. H. (1965) Potassium retention in montmorillonites: *Clay Minerals* **6**, 17–22. [Pergamon Press, New York].

Weir, A. H., and Greene-Kelly, R. (1962) Beidellite: *Am. Mineralogist* **47**, 137–46.

Weiss, A., Koch, G., and Hofmann, U., (1955) Zur Kenntnis von Saponite: *Ber. Deut. Keram. Ges.* **32**, 12–17.

Résumé—Une analyse radiographique d'échantillons saturés de Li^+ et de K^+, analyse différentielle thermique (DTA), analyse gravimetrique thermique (TGA), et analyse chemique de 83 échantillons permettent de faire une distinction entre Wyoming. Tatatilla, Otay, Chambers, et les types de montmorillonites non idéaux, et entre les types de beidellites idéaux et non idéaux. Le test Greene-Kelly Li^+ différencie les montmorillonites des beidellites. La redilation par éthylène glycol après saturation de K^+ et chauffage à 300°C, dépend de la charge de couche totale nette et non pas de l'emplacement de la charge. Les montmorillonites du type Wyoming sont caracterisées par une charge de couche nette relativement basse, elles ont pour propriété de se redilater à 17 A, alors que la plupart des autres montmorillonites et beidellites possèdent une charge de couche nette plus élevée et se redilatent à moins de 17 A.

Les écarts importants de température de déshydroxylation ne peuvent constamment se rapporter

https://doi.org/10.1346/CCMN.1969.0170302 Published online by Cambridge University Press

à la quantité de Al^{3+} pour la substitution de Si^{4+}, ni à la quantité des cations de couche intermédiaire du type Mg, Fe ou à la grosseur des particules. Le plus important facteur de contrôle de la température de déshydroxylation semble être la quantité de (OH) structurel. Des 19 échantillons analysés d'après le procédé d'analyse gravimétrique thermique (TGA), les montmorillonites et le beidellite idéal qui donnent des endothermes de déshydroxylation sur les courbes de l'analyse différentielle thermique (DTA) entre 650° et 760°C, contiennent tous à peu près la quantité idéale de 4(OH) par cellule unitaire. Les beidellites non idéaux contiennent plus que la quantité idéale de (OH) structurel et les montmorillonites non idéaux semblent en contenir moins, bien que la basse température de déshydroxylation de ces derniers puisse être causée par d'autres défauts de structure. Le changement d'intensité de la diffraction des rayons X de la réflexion 001 au cours de la déshydroxylation suggère que le supplément de (OH) des beidellites se produit au sommet des tétraèdres de SiO_4 ou AlO_4 avec le H^+ du (OH) polarisé vers les zones libres de cations de la feuille octaèdre.

Kurzreferat—Die Röntgenanalyse Li^+- und K^+-gesättigter Proben, die differentielle Thermoanalyse (DTA), die gravimetrische Thermoanalyse (GTA) und die chemische Analyse von 83 Proben ermöglicht es eine Unterscheidung zu treffen zwischen Wyoming. Tatatilla, Otay, Chambers und nichtidealen Typen von Montmorillonit, sowie zwischen idealen und nichtidealen Typen von Beidellit. Die Greene-Kelly Li^+-Prüfung unterscheidet zwischen Montmorilloniten und Beidelliten, Wiedererweiterung durch Äthylenglykol nach K^+ Sättigung und Erwärmung auf 300° hängt von der Gesamtschichtladung und nicht vom Ort der Ladung ab. Die Wyoming-Typ Montmorillonite haben charakteristisch niedrige Schichtladungen und erweitern sich erneut auf 17 Å, während die meisten anderen Montmorillonite und Beidellite eine höhere Schichtladung aufweisen und sich auf weniger als 17 Å erweitern.

Grössere Unterschiede in der Dehydroxylierungstemperatur können auf konsequente Weise weder zu dem Ausmass des Al^{3+} gegen Si^{4+} Austausches, noch zu der Menge von Mg, Fe, dem Typ der Zwischenlagenkationen oder der Teilchengrösse in eine Beziehung gebracht werden. Der hauptsächlichste, die Temperatur der Dehydroxylierung beeinflussende Faktor scheint die Menge des (OH) im Gefüge zu sein. Von den 19 durch TGA untersuchten Proben von Montmorilloniten und dem einen Beidellit, die auf ihren DTA Kurven Dehydroxylierungsendotherme zwischen 650° und 760°C ergeben, enthalten alle beinahe die ideale Menge von 4 (OH) pro Einheitszelle, die nichtidealen Montmorillonite und Beidellite, die Dehydroxylierungsspitzen zwischen 550° und 600°C ergeben, jedoch nicht. Nichtideale Beidellite enthalten mehr als die ideale Menge von (OH) im Gefüge, während die nichtidealen Montmorillonite weniger zu enthalten scheinen, obwohl die niedrige Dehydroxylierungstemperatur der letzteren auch auf andere Gefügefehler zurückzuführen sein könnte. Die Veränderung in der Röntgenbeugungsintensität der 001 Reflexion während der Dehydroxylierung deutet darauf hin, dass die zusätzlichen (OH) des Beidellits am Scheitel der SiO_4 oder AlO_4 Tetraeder vorkommen, wobei die H^+ der $(OH)^-$ gegen leere Kationenstellen in der oktaedrischen Platte hin polarisiert sind.

Резюме—Рентгеновское изучение образцов, насыщенных Li и K^+, дифференциальный термический анализ (ДТА), термогравиметрический анализ (ТГА) и данные химических анализов 83 образцов позволяют установить различие между монтмориллонитами из Вайоминга, Тататилла, Отэй и Чеймберса, монтмориллонитами неидеального типа и бейделлитами идеального и неидеального типов.

Насыщение Li^+, предложенное Грин-Келли, позволяет отличать монтмориллониты от бейделлитов. Набухание, которое вызывает этилен-гликоль после насыщения K^+ и нагревания до 300°C, зависит от полной величины заряда слоя, но не от его положения: монтмориллониты вайомингского типа отличаются низкой величиной заряда слоя и при набухании их $d_{(001)}$ возрастает до 17 А; у большинства других монтмориллонитов и бейделлитов заряд слоя больше, при набухании их $d_{(001)}$ не достигает 17 А. Основные различия в температурах дегидроксилизации не обнаруживают строгой зависимости как от количества Al^{3+}, замещающего Si^{4+}, так и от количества Mg, Fe, типа межслоевых катионов, величины частиц. Главным фактором, контролирующим температуру дегидроксилизации, по-видимому, является количество структурных (OH). Из 19 изученных с помощью ТГА образцов все монтмориллониты и один идеальный бейделлит, давшие на кривых ДТА эндотермические прогибы дегидроксилизации между 650 и 760°C, содержат почти идеальное количество гидроксилов—4 (OH) на элементарную ячейку. В этом отношении они отличаются от неидеальных монтмориллонитов и бейделлитов, которые дают прогиб дегидроксилизации между 550° и 600° С: неидеальные бейделлиты содержат больше, а неидеальные монтмориллониты меньше структурных (OH), чем идеальные; причиной низкой температуры дегидроксилизации неидеальных монтмориллонитов могут быть их другие структурные дефекты. Изменение интенсивности рефлекса (001) на рентгенограммах во время дегидроксилизации служит указанием на возможность того, что дополнительный (OH) бейделлита находится на вершине тетраэдров SiO_4 или AlO_4, причем H^+ в группе $(OH)^-$ ориентирован по направлению к вакантным позициям катионов в октаэдрическом слое.

https://doi.org/10.1346/CCMN.1969.0170302 Published online by Cambridge University Press